**HAL**
open science

# Magnetosheath-cusp interface

S. Savin, L. Zelenyi, S. Romanov, I. Sandahl, J. Pickett, E. Amata, L. Avanov,
J. Blecki, E. Budnik, J. Büchner, et al.

## HAL Id: hal-00329296
## https://hal.science/hal-00329296

Submitted on 18 Jun 2008

Annales
Geophysicae

# Magnetosheath-cusp interface

**S. Savin**[1], **L. Zelenyi**[1], **S. Romanov**[1], **I. Sandahl**[2], **J. Pickett**[13], **E. Amata**[6], **L. Avanov**[1], **J. Blecki**[9], **E. Budnik**[1],
**J. Büchner**[10], **C. Cattell**[15], **G. Consolini**[6], **J. Fedder**[11], **S. Fuselier**[7], **H. Kawano**[4], **S. Klimov**[1], **V. Korepanov**[16],
**D. Lagoutte**[12], **F. Marcucci**[6], **M. Mogilevsky**[1], **Z. Nemecek**[8], **B. Nikutowski**[10], **M. Nozdrachev**[1], **M. Parrot**[12],
**J. L. Rauch**[12], **V. Romanov**[1], **T. Romantsova**[1], **C. T. Russell**[5], **J. Safrankova**[8], **J. A. Sauvaud**[14], **A. Skalsky**[1],
**V. Smirnov**[1], **K. Stasiewicz**[3,9], **J. G. Trotignon**[12], and **YU. Yermolaev**[1]

[1]Space Research Institute, Russian Academy of Sciences, Profsoyuznaya 84/32, Moscow, 117810, Russia
[2]Swedish Inst. Space Physics, Kiruna, Sweden
[3]Swedish Inst. Space Physics, Uppsala, Sweden
[4]Kyushu University, Japan
[5]IGPP, UCLA, USA
[6]Interplanetary Space Phys. Inst., CNR, Roma, Italy
[7]Lockheed Martin Alto Res. Lab., CA, USA
[8]Faculty Math. Phys., Charles U., Praha, Czech Republic
[9]Space Res. Center, Polish Academy Sci., Warsaw, Poland
[10]Max-Planck Inst. Aeronomie, Katlenburg-Lindau, Germany
[11]Naval Research Lab., Washington, USA
[12]Laboratory Phys. Chemistry Environment, Orleans, France
[13]University of Iowa, USA
[14]Centre d'Etude Spatiale des Rayonnements, Toulouse, France
[15]University of Minnesota, USA
[16]Lviv Center for Space Researches, Ukraine

**Abstract.** We advance the achievements of Interball-1 and other contemporary missions in exploration of the magnetosheath-cusp interface. Extensive discussion of published results is accompanied by presentation of new data from a case study and a comparison of those data within the broader context of three-year magnetopause (MP) crossings by Interball-1. Multi-spacecraft boundary layer studies reveal that in ∼80% of the cases the interaction of the magnetosheath (MSH) flow with the high latitude MP produces a layer containing strong nonlinear turbulence, called the turbulent boundary layer (TBL). The TBL contains wave trains with flows at approximately the Alfvén speed along field lines and "diamagnetic bubbles" with small magnetic fields inside. A comparison of the multi-point measurements obtained on 29 May 1996 with a global MHD model indicates that three types of populating processes should be operative:

– large-scale ($\sim$few $R_E$) anti-parallel merging at sites remote from the cusp;

– medium-scale (few thousand km) local TBL-merging of fields that are anti-parallel on average;

– small-scale (few hundred km) bursty reconnection of fluctuating magnetic fields, representing a continuous mechanism for MSH plasma inflow into the magnetosphere, which could dominate in quasi-steady cases.

The lowest frequency ($\sim$1–2 mHz) TBL fluctuations are traced throughout the magnetosheath from the post-bow shock region up to the inner magnetopause border. The resonance of these fluctuations with dayside flux tubes might provide an effective correlative link for the entire dayside region of the solar wind interaction with the magnetopause and cusp ionosphere. The TBL disturbances are characterized by kinked, double-sloped wave power spectra and, most probably, three-wave cascading. Both elliptical polarization and nearly Alfvénic phase velocities with characteristic dispersion indicate the kinetic Alfvénic nature of the TBL waves. The three-wave phase coupling could effectively support the self-organization of the TBL plasma by means of coherent resonant-like structures. The estimated characteristic scale of the "resonator" is of the order of the TBL dimension over the cusps. Inverse cascades of kinetic Alfvén waves are proposed for forming the larger scale "organizing" structures, which in turn synchronize all nonlinear cascades within the TBL in a self-consistent manner. This infers a qualitative differ-

*Correspondence to:* S. Savin (ssavin@iki.rssi.ru)

ence from the traditional approach, wherein the MSH/cusp interaction is regarded as a linear superposition of magnetospheric responses on the solar wind or MSH disturbances.

**Key words.** Magnetospheric physics (magnetopause, cusp, and boundary layers) – Space plasma physics (turbulence; nonlinear phenomena)

## 1 Introduction and definitions

The International Solar-Terrestrial Physics (ISTP) program provides wide opportunities for study of the penetration of magnetosheath (MSH) plasma into the magnetosphere by means of multi-point observations. In this paper we present a case study, using data from several ISTP satellites, and briefly compare them with three-year Interball-1 maps of high-amplitude magnetic fluctuations in the magnetopause (MP) vicinity. Then both the presented and the published results of exploration of the MSH-cusp interface are widely discussed.

Early single spacecraft observations with Heos-2 and later Prognoz-7, 8, 10 have shown that the MP position and magnetosheath plasma flow structures are quite variable near the cusp, a magnetospheric region that is crucial for magnetosheath plasma entry (Paschmann et al., 1976; Haerendel and Paschmann, 1975; Klimov et al., 1986; Lundin et al., 1991; Savin, 1994). Because of differences in the data, researchers have divided the high altitude cusp into a number of layers and regions. Since full agreement on how this should be done is not yet achieved, we will give the definitions and descriptions of the regions discussed in this paper. These regions, shown in Plate A1, are: the outer and inner cusps, the outer cusp throat (OT) and the turbulent boundary layer (TBL). The reader is referred to the papers by Smith and Lockwood (1996) and Angelopoulos et al. (2001) for a synopsis of measurements and models of the low altitude cusp.

Referring to Plate A1, the outer cusp throat (pink slant-line shaded region) is outside the MP, the outer cusp (light blue) is just inside the MP, and the inner cusp is deeper in the magnetosphere. We identify here the MP (inner red line) as the innermost current sheet, where the magnetic field turns from Earth-controlled to magnetosheath-controlled (Haerendel and Paschmann, 1975). The outer cusp is a region with three different particle populations: newly-injected MSH ions, MSH ions reflected from the ionosphere, and quasi-perpendicular ions trapped in the local magnetic field minimum near the cusp (Savin et al., 1998b; Sandahl et al., 2000). There are also electrons accelerated along the field lines. The newly-injected and quasi-perpendicular ions dominate over those that are reflected. This is one of the characteristics distinguishing the outer cusp from the inner cusp and from the distant mantle. The outer cusp is also characterized by moderate magnetic noise, while in the inner cusp there is a similar type of noise observed primarily only at the boundaries (Pottelette et al., 1990). The outer cusp consists of the entry
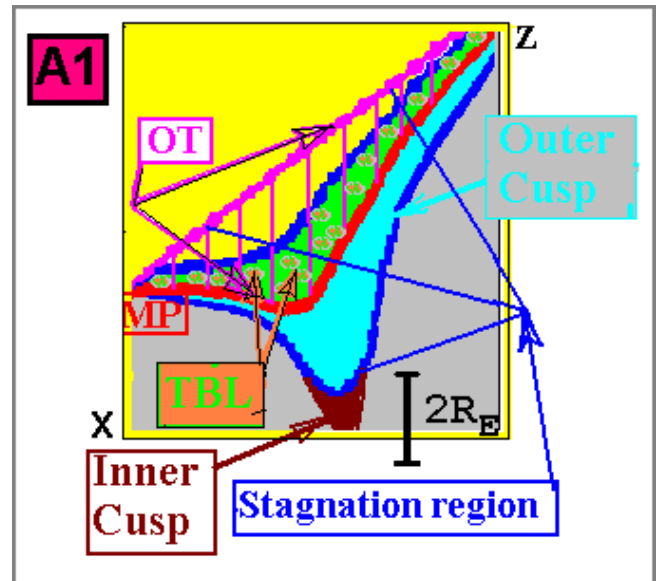


**Plate A1.** Characteristic regions at the magnetosheath-cusp interface for the noon meridian plane in the summer period (i.e. for the positive dipole tilt): the inner and outer (OC) cusps, the outer cusp throat (OT), stagnation region, magnetopause (MP) and the turbulent boundary layer (TBL). See also the text for more details.

layer and the portion of the plasma mantle adjoining the entry layer (Paschmann et al., 1976). According to the work of Yamauchi and Lundin (1997) the entry layer and mantle that are parts of the outer cusp form one continuous region.

At the cusp the magnetopause can be indented. This indentation was first predicted by Spreiter and Briggs (1962) and then detected by HEOS-2 (Paschmann et al., 1976), ISEE (Petrinec and Russell, 1995), and Hawkeye-1 (Chen et al., 1997). Zhou and Russell (1997) found that the MP is closer to the Earth at high latitudes than at low latitudes. Interball-1 statistics show that the indentation is on the average about $2 R_E$ deep (Savin et al., 1998b). We call this part of the exterior cusp the outer cusp throat (OT). The plasma in the outer cusp throat is highly disturbed and/or stagnant MSH plasma. The difference between our outer cusp throat and the "stagnation region" defined by Haerendel et al. (1978) is that the stagnation region has no specific relation to the magnetopause, as noted by the multiple arrows in Plate A1. Usually, the magnetopause can be recognized in both Polar and Interball-1 data, but when this is not the case, it is better to use the term "stagnation region", rather than "outer cusp throat".

The turbulent boundary layer (TBL) is a region dominated by irregular magnetic fields and plasma flows. It is located just outside and/or at the near cusp magnetopause, and has recently been found to be a permanent feature (Savin et al., 1997, 1998b, 2002a; Klimov et al., 1997; Sandahl et al., 2000). Here the energy density of the ultra low frequency (ULF) magnetic fluctuations is comparable to the ion kinetic, thermal, and DC magnetic field densities. The ULF power is usually several times larger than that in the MSH, and one or
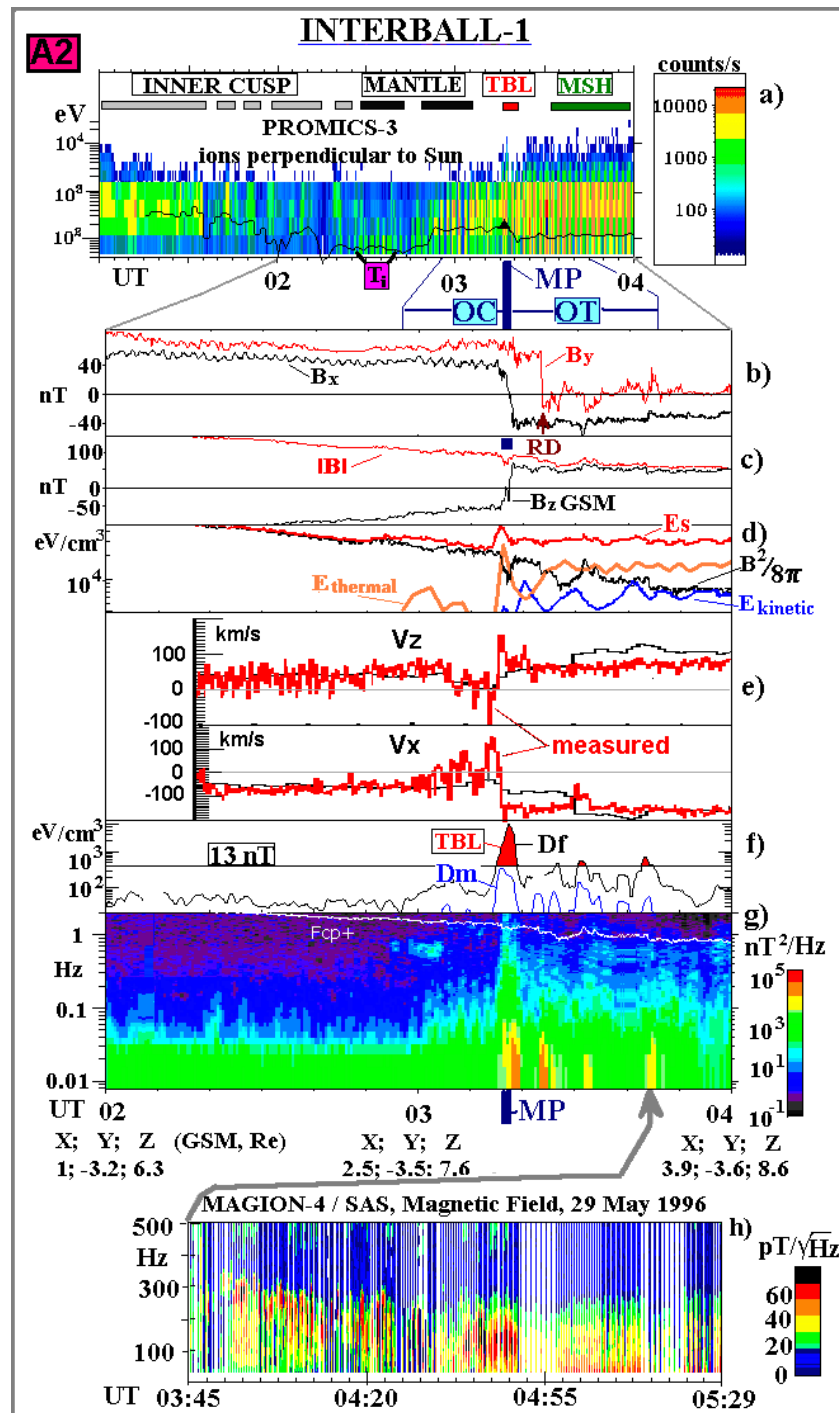
**Plate A2.** Outbound MSH/cusp interface crossing by Interball-1 and Magion-4 on 29 May 1996. The regions depicted in Plate A1 are marked at the top of panels (a), (b). Panel (**a**): energy distribution of the protons perpendicular to the Sun-Earth line (PROMICS-3); the ion temperature $T_i$ is depicted by a black line. Panels (**b**) and (**c**): magnetic field in the GSM coordinates. Panel (**d**): the total energy density, $Es$ (red), the thermal energy density, $E_{thermal}$ (brown), the kinetic energy density, $E_{kinetic}$ and the magnetic energy density, $Em = B^2/8\pi$ (black). Panel (**e**): GSE $V_x$ and $V_z$ components of ion velocity from the MHD model of Fedder et al. (1995) (black trace) and measurements by SKA-1 ion spectrometer (red colored). Panel (**f**): the power in the magnetic field variations, $Df$, and the standard deviation of the magnetic field magnitude, $Dm$ (blue). Panel (**g**): Fourier spectrogram of the magnetic field power with sampling rate 4 Hz; the proton cyclotron frequency labeled "Fcp+" is over-plotted by a white line. Panel (**h**): magnetic spectra from Magion-4 in the range 20–2000 Hz during a period when Interball-1 observed the upstream turbulence.
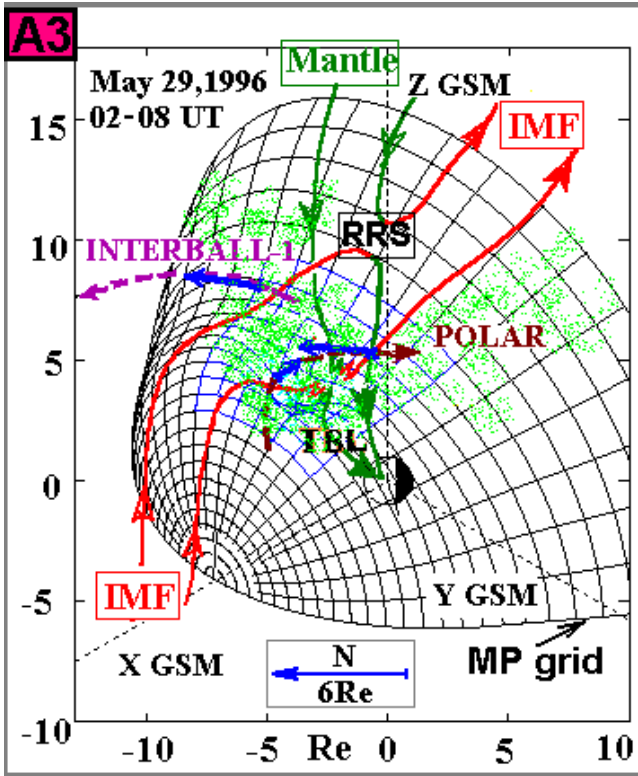
**Plate A3.** Sketch for reconnection at the indented magnetopause during northward IMF conditions on 29 May 1996. The black magnetopause (MP) grid is described in Sect. 6.2. Polar and Interball-1 orbits are shown by the dashed brown and violet lines, respectively. The TBL from Fig. 8 is depicted by green dots. The measured MP normals are marked by blue arrows (the total normal length is shown at the bottom of the figure by a blue arrow marked by "N"). The draped IMF magnetic field lines are marked by a red color, the magnetospheric/ mantle lines – by a green color.



**Plate A4.** The distribution of the currents perpendicular to the magnetic field in the noon meridian plane in SM coordinates depicted by the color scale from the global MHD model by Fedder et al. (1995). The projections of the Polar (brown trace) and Interball-1 (black trace) orbits onto that plane (Polar crossed this plane at 05:30 UT) are also shown. The dayside magnetopause (MP) and bow shock (BS) are seen in the current maxima at low latitudes, the higher latitude smooth MP from Sibeck et al. (1991) model is depicted by the violet line. The global MHD model determined "remote" (from the cusp) reconnection site (RRS) position is shown by a white squared cross. The model inward boundary of the MSH plasma with density >40/cc is shown by a thick black-and-white dashed line (see also Fig. 7 in Russell et al., 1998).

two orders of magnitude larger than that inside the magnetopause. As recent studies conclude (see, e.g. Belmont and Rezeau, 2001 and references therein) the strong ULF fluctuations that occur just outside of or at the magnetopause can independently result in micro-reconnection and local plasma penetration all along the magnetopause surface even without the presence of quasi-stationary global reconnection. In two case studies Savin et al. (1998b) have shown that large-scale structures (>30 s) tend to be spatial, while for shorter time scales the temporal changes are significant. In this paper we do not separate the spatial changes from the temporal variations. We utilize the magnetic AC power related to the average plasma and field energy density in the magnetosheath as a rough measure of the strong turbulence regime. This ratio being >0.1 corresponds to strong diffusion discussed in the percolation theory of Kuznetsova and Zelenyi (1990). Haerendel (1978) was the first to introduce the turbulent boundary layer in cusp physics in a discussion on the interaction of the magnetosheath flow with the magnetopause at the flank of the tail lobe. Examples of highly turbulent magnetic and electric fields in the exterior cusp have been reported by
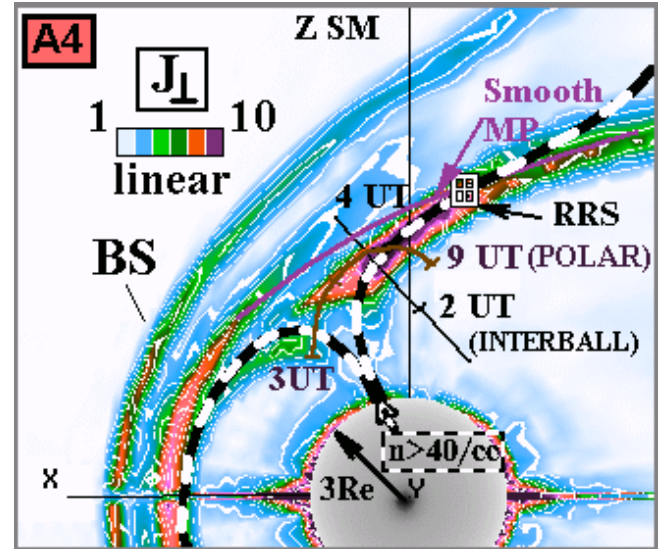
Paschmann et al. (1976) and Haerendel et al. (1978) from Heos-2, by Klimov et al. (1986) from Prognoz-10, by Savin (1994) and Blecki et al. (1998), from Prognoz-8 and by Chen et al. (1997) from Hawkeye-1 data, but the referenced papers dealt neither with the turbulent boundary layer statistics nor with multi-satellite data. Only the Prognoz-8 and 10 magnetic field experiments had a high enough sampling rate (1–50 Hz versus ∼0.03 Hz on Heos-2 and Hawkeye-1) for turbulent boundary layer studies. However, the absence of 3-D plasma measurements and poor statistics prevented a systematic study of the turbulent boundary layer signatures and of the TBL's role in mass and momentum transport at the high latitude magnetopause.

The main goal of this paper is to advance the achievements and to explore solutions to the problems associated with the physics of the exterior cusp in the Interball era. At the same time, we have significant amounts of original results from recent analyses of multi-spacecraft data, which are obviously beyond the scope of a single paper. Thus, as a compromise, we limit ourselves in the data presentation to a fortunate multi-point case and a consideration of that case in the context of three-year Interball-1 operation. The case study presented in this paper deals with the dayside cusp and magnetosheath interface during dominant north-
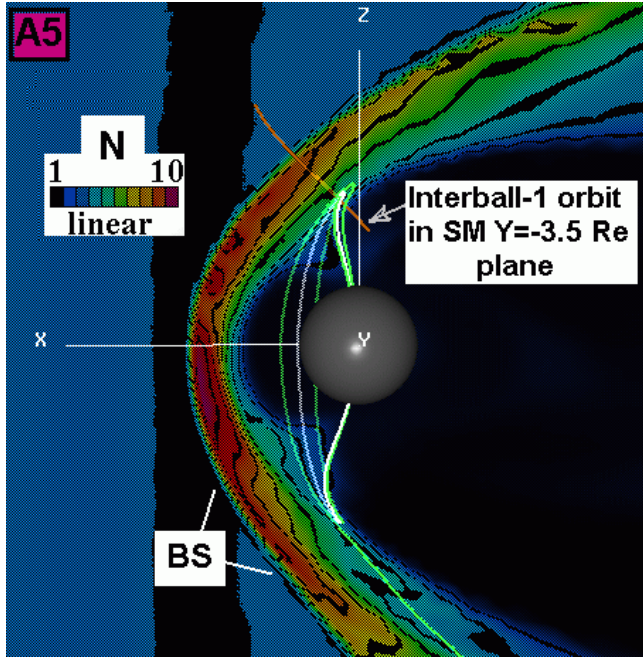
**Plate A5.** The plasma density from the global MHD model by Fedder et al. (1995) on the $Y = -3.5\,R_E$ plane and field lines through Interball orbit at 03:14 UT (white) and $\pm 0.25\,R_E$ around the central field line (green). The MSH corresponds to the density maximum between the BS and empty magnetosphere. On the closed magnetospheric lines (white and inner green ones) density enhancements are seen sunward of these kinked lines (which are mostly out of the semi-transparent density plane). The green field line farthest from the Earth is the reconnected one.

ward IMF conditions. We discuss examples of the characteristic regions at the cusp/MSH interface on the basis of the data from Interball-1 and Polar on 29 May 1996 and compare them with results of global MHD modeling of the solar wind interaction with the magnetosphere. There are a number of previous studies of this event, but they have concentrated on single spacecraft data (see, e.g. Russell et al., 1998; Savin et al., 1998a; Chandler et al., 1999; Avanov et al., 2001). In our study Interball-1 serves as the upstream MSH monitor for Polar in the TBL and for HEO-095 and DMSP in the inner cusp (see Grande et al., 1997) and ionosphere, respectively. We also add wave data to distinguish different regions and phenomena. One of the main questions we address here is whether the TBL plays a substantial role in MSH plasma penetration into the magnetosphere. We make use of the spacecraft fleet data and event-oriented modeling to determine if the anti-parallel magnetic field merging (either local or remote from the cusp) is able to account for the widespread cusp, detected on this day, from the ionosphere to the magnetopause over a wide range of local times. We compare the presented case with maps of the high level of ULF magnetic turbulence (i.e. of the TBL) on the basis of the three years of Interball-1 data. The comparison provides background both for the case study that is presented and for other cases discussed throughout the paper. In the second part of our pa-

per we summarize the TBL properties, as known up to this point in time, and discuss three types of reconnection that are proposed to occur at different scales. We consider percolation of the MSH plasma as a source for the cusp and boundary layers. We compare the direct interaction of MSH flows with the indented MP over the cusp with reconnection as an alternative source for the TBL. A scenario for three-wave resonance-like interactions in the TBL is proposed. We treat the high-latitude MP as a nonlinear distributed system with memory.

## 2 Description of event and methodology used

We start from an event of multi-spacecraft constellation in the northern cusp and at its outer border on 29 May 1996. In our presentation Plates A1–A5 depict Interball observations and their analysis using the global MHD simulation results. Plates B1–B5 deal with Polar observations and their interpretation using wavelet analysis techniques.

### 2.1 Event description

In Plates A2 and B1 we present multi-instrument Interball-1, Magion-4 and Polar data on 29 May 1996. In Plates A3-A5 one can see the Interball-1 and Polar orbits relative to the cusp-MSH interface, the details of which are discussed below. The top panel (a) of Plate A2 shows protons perpendicular to the satellite spin axis and Sun-Earth line measured by the PROMICS-3 instrument; the ion temperature $T_i$ is overplotted by a black line. Panels (b) and (c) show the magnetic field in the GSM coordinate system, $B_y$ and $|\boldsymbol{B}|$ are plotted by red lines, $B_x$ and $B_z$ – by black lines. Panel (d) gives the different components of the energy density; the total energy density, $Es$ (red line), and its three components, the thermal energy density, $E_{\text{thermal}} = 1.5\,nkT_i$ (brown line, where $n$ – plasma density, $T_i$ – ion temperature), the kinetic energy density, $E_{\text{kinetic}} = 0.5nM_iV_i^2$ (blue line, where $M_i$ and $V_i$ – ion mass and velocity) and the magnetic energy density, $Em = \boldsymbol{B}^2/8\pi$ (black line). Panel (e) displays GSE $V_x$ and $V_z$ components of ion velocity from the MHD model of Fedder et al. (1995) (black trace, see Sect. 2.2) and measurements by SKA-1 ion spectrometer (see details of the plasma data in Avanov et al., 2001), which are colored red. Panel (f) shows the power contained in the magnetic field variations, $Df$, and the standard deviation of the magnetic field magnitude, $Dm$. $Df$ is obtained by taking the sum of variation powers in $B_x$, $B_y$ and $B_z$. Then we use the relation $1\,\text{eV} \sim 2.49\,\text{nT}^2$ to express $Df/Dm$ in energy density units. The variations are calculated over two-minute intervals with the interval shifts of 30 s. Panel (g) gives a Fourier spectrogram of the magnetic field with sampling rate 4 Hz and the proton cyclotron frequency (white line). Finally, panel (h) shows magnetic spectra from Interball-1's companion satellite, Magion-4, in the range 20–2000 Hz during a period when Interball-1 observed turbulence upstream of the MP. The different regions depicted in Plate A1, which were
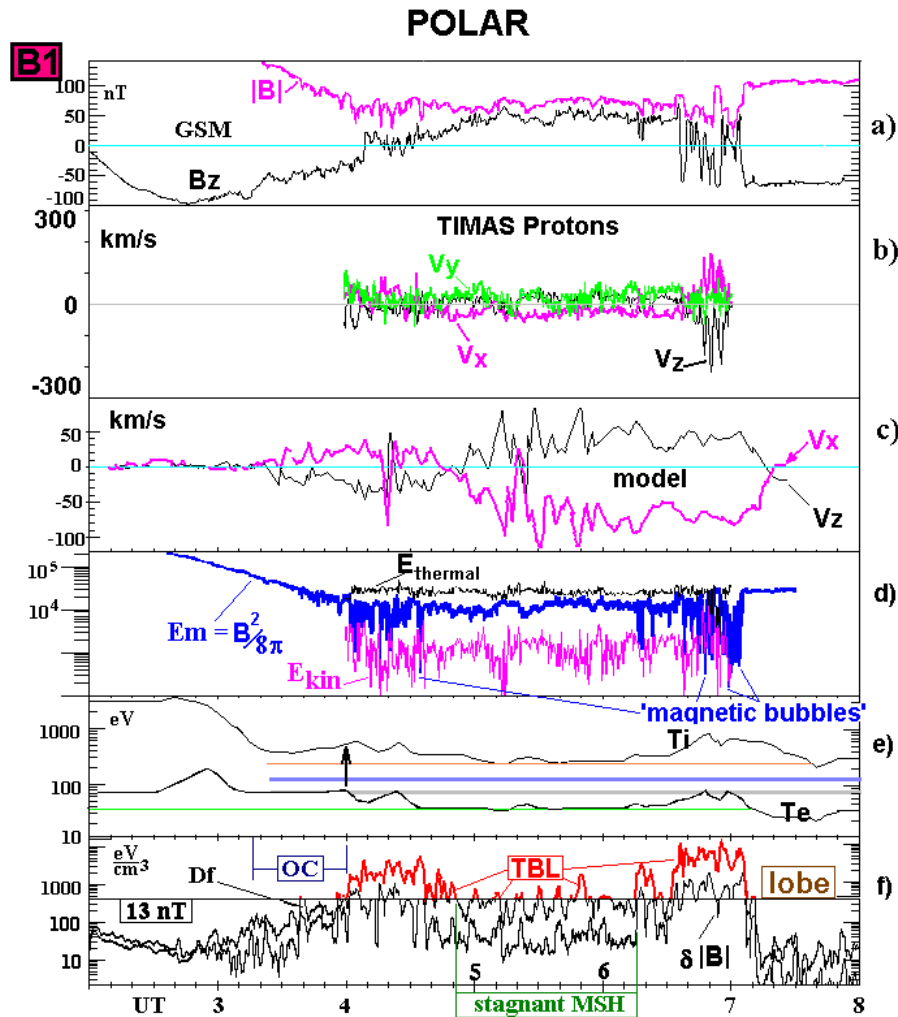
## POLAR



**Plate B1.** Particle and field parameters on Polar on 29 May 1996. Panel **(a)**: the magnetic field $|\mathbf{B}|$ (violet) and GSM $B_z$ (black). Panel **(b)**: vector velocities of protons by the TIMAS spectrometer, $V_x$, $V_y$ and $V_z$ are marked by violet, green and black colors, respectively. Panel **(c)**: GSM $V_x$ (violet) and $V_z$ (black) components of ion velocity from the global MHD model (Fedder et al., 1995). Panel **(d)**: the kinetic ion energy density (violet), the ion thermal energy density (black), and the magnetic energy density (blue); the ion densities are shown only at 04:00–07:00 UT. Panel **(e)**: the average ion energy $T_i$ (upper black line) from HYDRA, the minimum $T_i$ from Polar in the MSH (brown), the characteristic $T_i$ in the MSH from Interball-1 (thick blue line) at 04:00 UT (marked by the vertical arrow), $T_i$ in the MSH from the MHD model at 04:00 UT (gray line), average electron energy $T_e$ (the lower black line) from HYDRA, and minimum $T_e$ in the MSH / TBL (green). Panel **(f)**: the magnetic field variations calculated in the same way as on panel (f) of Plate A2; the TBL is red-colored in $Df$, upper curve, the characteristic regions marked according to Plate A1.

passed by Interball-1, are marked at the top of Plate A2. Until 02:20 UT Interball-1 was in the inner cusp. At ∼02:30 UT the mantle was encountered. Particle fluxes were fairly weak and had no earthward component (not shown). The outer cusp (OC) boundary was approached at about 03:00 UT, which is indicated by increased particle fluxes and wave activity. At 03:17 UT the MP was crossed. This can be determined here from the sign change in $B_z$, which went from negative inside the magnetosphere to positive in the outer cusp throat (OT). The sign of $B_x$ also changed. At the magnetopause current sheet the thermal energy density was the main component in the total energy density, while there was a dip in the magnetic energy density. The period from 03:15 to

03:19 UT represents a typical example of a turbulent boundary layer at the OT edge. At 03:17 UT in Plate A2 maxima are seen, in $T_i$ (marked by black shadowing), thermal and total energy densities and magnetic field spectra. A characteristic feature of the TBL is the dominance of incompressible waves resulting from the fact that total wave power, $Df$, is several times higher than the magnetic field magnitude standard deviation $Dm$ (the lower curve on panel (f); cf. Savin et al., 1998b). The total energy density measured in the magnetosheath outside the cusp was about 30 keV/cm$^3$, the magnetic wave power in the TBL reached 6 keV/cm$^3$ and thus, the ratio between the two was $Df/Es \sim 0.2$ (i.e. exceeds the strong turbulence limit of 0.1, see previous section).
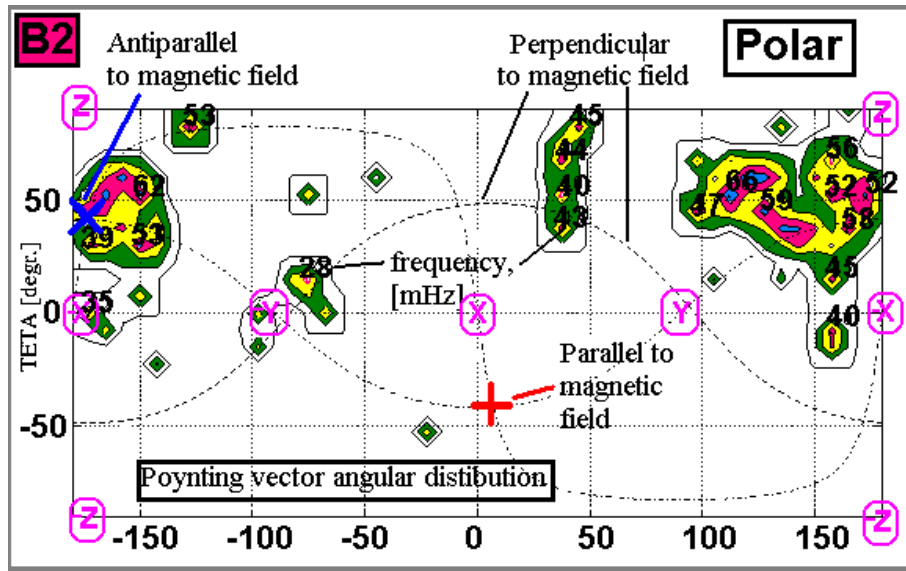
**Plate B2.** 07:00:00–07:01:56 UT: angular distribution of the Poynting flux in GSM coordinates from Polar; median frequency of the maximums is given in mHz (see details in text).
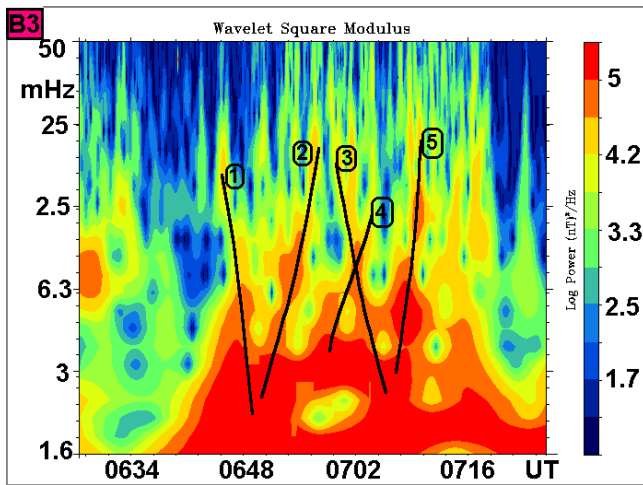


**Plate B3.** Wavelet spectrogram ($B_z$ SM): Polar TBL (see Plate B1), numbered black lines mark the inferred wave cascades (2, 4, 5 – direct cascades, 1,3 – inverse cascades, see text for further details).
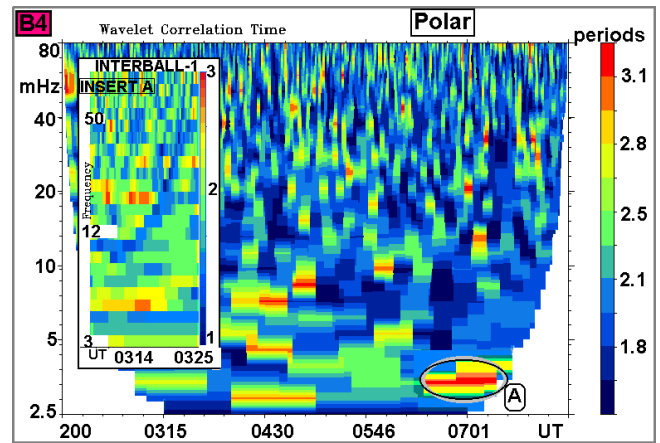


**Plate B4.** Wavelet correlation time for SM $B_z$ from Polar in the TBL (see Plates B1 and B3). Label 'A' stands for the coherent structure depicted in Plate B3. Figure 1: the same for Interball-1 GSM $B_y$ (see text for further details).

Polar data are presented in Plate B1. Panel (a) shows the magnetic field ($B_z$ by black line, $|\boldsymbol{B}|$ by violet line); panel (b) shows vector velocities from the moments of measurements of protons by the TIMAS spectrometer. Panel (c) displays GSM $V_x$ and $V_z$ components of the ion velocity from the model (see Sect. 3 and Fedder et al., 1995 for details). On panel (d) we depict the ion kinetic energy density, $E_{kin} = 0.5nM_iV_i^2$ (black line, where $M_i$ and $V_i$ – ion mass and velocity), the thermal energy density, $E_{\text{thermal}} = nk(T_\perp + T_{par}/2)$ (black line, where $n$ – plasma density, $T_\perp$ and $T_{par}$ – perpendicular and parallel proton temperatures from TIMAS), and the magnetic energy density, $Em = \boldsymbol{B}^2/8\pi$ (blue line). Panel (e) gives the average ion

energy, $T_i$, and average electron energy, $T_e$, from HYDRA. Panel (f) shows the magnetic field variations calculated in the same way as in panel (f) of Plate A2 ($Df$ – upper curve, $Dm$ – lower curve). The Polar data differ from those of Interball-1 in Plate A2 by extended duration crossings of the intensive part of the turbulent boundary layer. The TBL is seen as increases in the wave power, $Df$, of 8–40 times that of the stagnant MSH. The TBL threshold ($Df = 400$ eV/cc, $\sim$13 nT$^2$, see panel f) is about two times higher than $Df$ in the stagnant MSH. $Df \gg Dm$ displays strong dominance of the transverse waves over the compressible ones in the TBL.

On the Polar outbound leg there is a gradual rotation of the average field direction immersed in the high level TBL
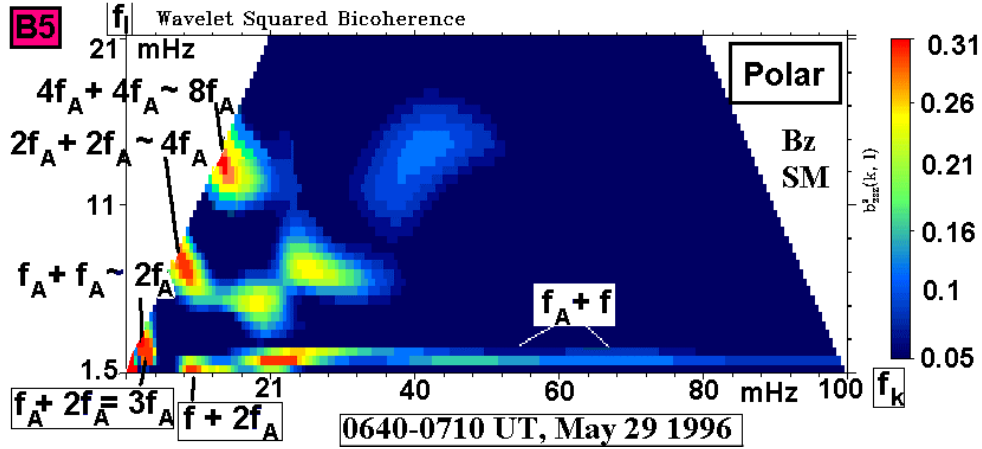
**Plate B5.** Wavelet bi-spectra from Polar for SM $B_z$ in the inbound TBL crossing at 06:40–07:10 UT on 29 May 1996 (cf. Plate B3 and Plate B4); the maximums correspond to 3-wave processes: $f = f_l + f_k$. The frequency $f_l \sim f_A$ corresponds to that labeled 'A' in Plate B4. $f_A + f_A = 2 f_A$, etc. corresponds to the harmonic generation (see also text).
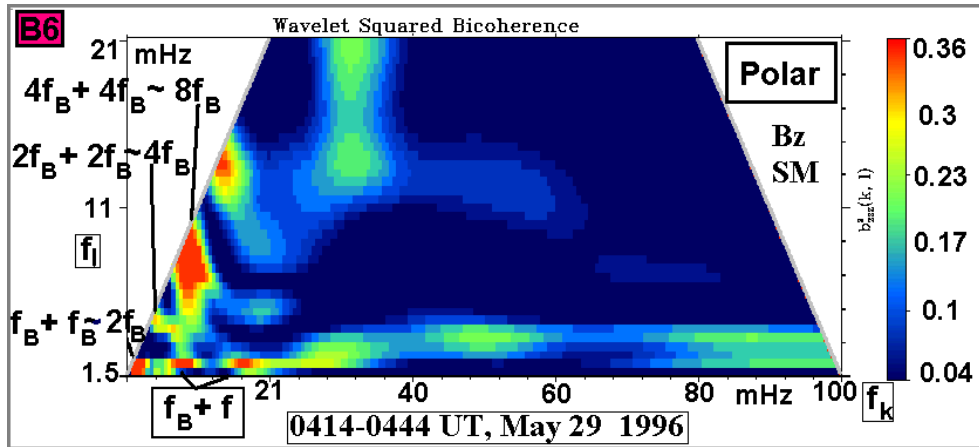


**Plate B6.** The same as for Plate B5 for the Polar outbound TBL crossing at 04:14–04:44 UT on 29 May 1996 (cf. Plate B3 and Plate B4).

(04:00–04:45 UT). The main MP current sheet at 04:08 UT is rather weak (see the $B_z$ change in panel a). In the TBL the wave power reaches 20% of the $E_{\text{thermal}}$ at 05:10 UT, or of the $Es$ from the simultaneous Interball-1 measurements in the MSH. The "magnetic bubbles" are identifiable by the spiky drops in $\boldsymbol{B}^2/8\pi$ and $|\boldsymbol{B}|$ (marked in Plate B1, panel d). $T_e$ and $T_i$ rise in the TBL by factors of 2–4 compared with their minimums at 05:00 UT (brown curve in Plate B1e), or with Interball-1 data at 04:00 UT (blue curve for $T_i$). The MHD model predicts an even lower $T_i$ value (gray curve) at this time (black arrow in Plate B1e). The TBL with a higher turbulence level is on the Polar inbound leg into the polar cap at 06:16–07:08 UT. $T_i$ raises a factor of 3–6 and $Df$ reaches 33% of the MSH $E_{\text{thermal}}$, which is $\sim Em$ (panels d and f) just inside the lobe (i.e. a pressure balance at the MP). In the "magnetic bubbles" $|\boldsymbol{B}|$ drops down to fractions of nT. Minimum $T_i$ is $\sim$2 times higher than that observed in both the unperturbed MSH at the same time and $\sim$3 times higher than that in the MHD model (see brown, blue and gray horizontal

lines in Plate B1e). This could result from heating both in the TBL (if the MSH plasma enters, then leaves the TBL) and/or at the interface between the streaming and stagnant MSH. Note also the remarkable wave train in the velocity at 06:40–07:00 UT data (panel (b) of Panel B1). We devote a special section to the detailed study of this period with the nearly Alfvénic velocity jets unpredicted by the MHD model. We will return to the detailed event analysis in Sect. 3.

## 2.2 Global MHD simulation

Results of the global MHD modeling for 29 May 1996 with the SW data as an input (see Fedder et al., 1995 for details) are presented in Plates A4, A5 and Fig. 7.

The distribution of the currents perpendicular to the magnetic field ($J_\perp$) in the noon meridian plane in SM coordinates is depicted in Plate A4 by the color scale. Also shown are the projections of the Polar and Interball-1 orbits onto that plane (Polar crossed this plane at 05:30 UT). The day-

side low latitude MP and bow shock (BS) are easily seen in the $J_\perp$ maximum, while at higher latitude the MP current splits into 3 branches. The sunward one, being an extension of the dayside depletion layer, might interfere with the MSH flow to reach the outer-cusp-throat dent (Savin et al., 1998a). It is difficult to say if the gap between the 3 current branches (just over the Polar orbit crossing with the "40/cc" boundary at ∼03:20 UT) provides direct access ("cleft") for the MSH plasma into the cusp. The current gradients near the spacecraft orbits should cause current drift instabilities (see e.g. Vaisberg et al., 1983 and references therein), that provide a source for the TBL waves (see Sect. 3.1). Note that the TBL crossings by Polar correspond to the $J_\perp$ maximum; the stagnant MSH encounter represents sliding along the current maximum border. The broadness of the maximum current sheet itself is believed to be due to MHD (= large scale >3000 km) waves, which are reproduced by the model. The MP indentation is seen as the lag between the "smooth MP" (see e.g. Sibeck et al., 1991 model) and the current sheet maximum. Its depth (∼1.5 $R_E$) is typical for the outer cusp throat (see Fig. 8a and Savin et al., 1998b). The model-determined position of the "remote" (from the cusp) reconnection site (RRS) is shown in Plate A4 by a white squared cross. We also mark it as "RRS" in Plate A3 (see the Sect. 6.2). The model inward boundary of the MSH plasma with density >40/cc is shown by a thick black-and-white dashed line (see Fig. 7 in Russell et al., 1998).

We present in Plate A5 the model plasma density on the $Y = -3.5\,R_E$ plane and field lines through the Interball orbit at 03:14 UT (white) and ±0.25 $R_E$ around the central field line (green). The −3.5 $R_E$ plane in the Plate is transparent so that the field lines are brighter when they are in front of the plane and are dimmer when they are behind the plane. The MSH is well depicted by the density maximum between the BS and the empty magnetosphere. On the closed magnetospheric lines (white and inner green ones) density enhancements are seen sunward of these kinked lines (which are mostly out of the semi-transparent density plane). Both the line shapes and location of these cusp-like density maxima indicate that the RRS is the general model source of the MSH plasma inside magnetosphere. Farther from the Earth the green field line is the reconnected one, the southern former-MSH part of which is draped over the southern cusp. Thus, the model predicts the crossing by Interball of the reconnected field line, originating from the remote reconnection site (at about the same place as the RRS in Plate A4). The model magnetic field satisfactorily reproduces the average measured one (Russell et al., 1998).

As we have mentioned in the Introduction, on 29 May 1996, the cusp has been sampled from the upper ionosphere up to the interface with the MSH. The MHD model serves to link the measurements at different altitudes relative to the RRS, remembering that the model is adjusted to the SW input. A representative summary picture of the cusp and BL encounters by 5 spacecraft, projected to the ionosphere, is depicted in Fig. 7 along with the RRS traces and characteristic equipotential patterns from global MHD simula-

tions in the coordinates invariant latitude and MLT in the Northern Hemisphere. From Fig. 7a one can see that the multi-spacecraft data provide the unprecedented wide coverage of the high latitude magnetic field lines in invariant latitude, MLT and UT. At lower altitudes the HEO 95-034 and DMSP F12 and F13 registered the cusp, shown by the thick blue lines (their traces have been calculated without usage of the MHD model, see Grande et al., 1997 for details). The crosses show projections of the reconnection locations from the global MHD model. Figure 7a demonstrates a wide cusp, the TBL (red thick lines) and an even mantle (green line) spread in MLT and UT. Figures 7b and 7c show the characteristic ionospheric equipotential patterns from the global MHD model; equipotential contours are plotted for cross-cap potential 6 kV and field-aligned current $4\,10^{-6}$ A/m. Note that the ionospheric convection is along the equipotential contours; the convection directions are displayed by the green arrows in the center and by the gray ones at the periphery. Traces of Polar (violet asterisks), Interball-1 (red circled triangle) and reconnection point footprints (brown arrow) are depicted as well. Figure 7b presents the main features of the MHD model convection up to 03:06 UT (inclusively). The global MHD model predicts Polar connection to the northern pole for the entire period, while Interball has no such connection starting from ∼03:20 UT, which is why it does not appear in Fig. 7c. The latter is in good correspondence with the Interball outbound MP at 03:17 UT in Plate A2 (see Sect. 2.1).

After the introduction of the MHD modeling results we will use the model as a guideline throughout the paper, especially in Sect. 4.

## 2.3 Wavelet analysis technique

Finally in the Sect. 2, we would like to describe the wavelet analysis techniques used in this paper in Plates B3–B6 and Figs. 3b and 5. Wavelet analysis is a powerful tool to investigate turbulent signals and short-lived structures. In order to examine the transient nonlinear signal in the TBL we have performed the wavelet transform with the Morlet wavelet:

$$W(a, t) = $$
$$C\Sigma\left\{f(t_i)\exp\left[i\,2\pi(t_i - t)/a - (t_i - t)^2/2a^2\right]\right\}, \quad (1)$$

where "$C$" has been chosen so that the wavelet transform amplitude $|W(a, t)|$ is equal to that of the Fourier transform (see Consolini and Lui, 2000 and references therein for details). This wavelet shows the single peak at the frequency $f = 1/a$, a wavelet characteristic scale may be read as representing a frequency $f = 1/a \pm f/8$. We use SWAN software from LPCE/CNRS in Orleans for the wavelet analysis. We apply this technique for Plate B3, Figs. 3b and 5.

To investigate the wave train coherence we utilize the wavelet correlation time. For that calculation the wavelet coefficients are considered, at every frequency, as a time history signal. This corresponds to the output of a low bandwidth filter centered on the analyzing frequency. A correlation analysis is performed over these new signals, taking
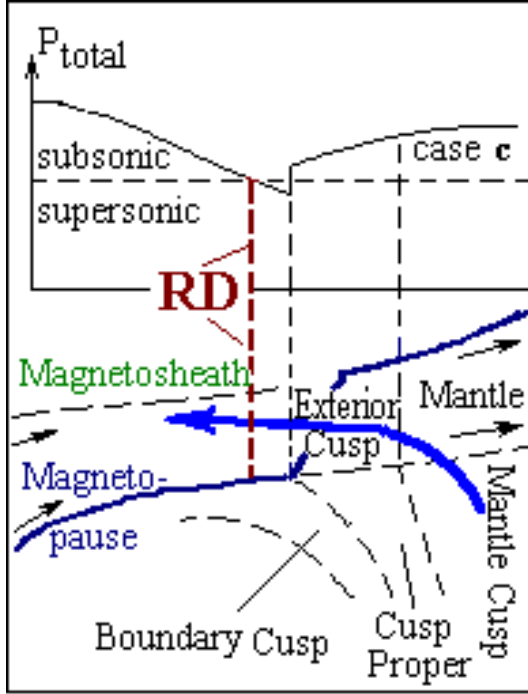
**Fig. 1.** Yamauchi and Lundin (1997) "Laval nozzle" model sketch; thick arrow infers Interball-1 orbit (see Plate A2). See text for further details.

into account a possible non-stationarity of the signals. The input series is the time variation of the wavelet coefficients $C(k, m)$. The function depends on the beginning time of the analysis $t$. At every discrete frequency $m$, the correlation function $R_c(t_i, l, m)$ is computed on a small moving time window:

$$R_c(t_i, l, m) = 1/Nl \sum_{n=iNl}^{(i+1)Nl-l-1} (C(n, m) - \mu c)(C(n+l, m) - \mu c)^*, 0 < l < l\,\mathrm{max}$$

where $N$ is the number of samples used to compute the correlation function and $l$ max is the maximum number of lags. The variable $\mu c$ is the mean value of the coefficients and $*$ means the complex conjugate operation. An overlapping of time intervals can be done. The correlation time is then estimated by the relation:

$$\tau c(t_i, m) = \gamma / T f \sum_{l=0}^{l\mathrm{max}} |R_c(l, m)| / R_c(0, m),$$

where $T_f$ is the period of the analyzed frequency ($T_f = 1/f$). Then, the result is expressed in terms of the number of periods (by selection of appropriate $\gamma$). We will return to the correlation time in the discussion of Plate B4 in Sect. 3.2.

We will do a further test for possible self-organization in the TBL processes by the usage of the wavelet-based bicoherence to check if the wave trains at different frequencies really constitute the coherent interactive system with multi-scale features. In the SWAN software the bicoherence is defined as:

$$b^2(a_1, a_2) = |B(a_1, a_2)|^2 / \left\{ \Sigma |W(a_1, t_i) W(a_2, t_i)|^2 \Sigma |W(a, t_i)|^2 \right\}, (2)$$

with $B(a_1, a_2)$ being the normalized squared wavelet bispectrum:

$$B(a_1, a_2) = \Sigma W^*(a, t_i) W(a_1, t_i) W(a_2, t_i). \quad (3)$$

The $W(a, t)$ is the wavelet transform defined by Eq. (2) and the sum is performed satisfying the following rule:

$$1/a = 1/a_1 + 1/a_2 \quad (4)$$

which corresponds to a frequency sum rule for the 3-wave process, $f = f_1 + f_2$.

The bicoherence has substantial value if three processes, with the highest frequency being the sum of the other two, are phase-coupled (cf. Consolini and Lui, 2000). The simplest such case is the harmonic generation due to quadratic nonlinearity, namely the second harmonic generation with $2f = f + f$, the third harmonic with $3f = 2f + f$, etc. The harmonics are present in any nonlinear wave pulse and do not represent phase coupling of the different waves. We assume that the dominant nonlinear process in the TBL is 3-wave decay (or junction) as the most powerful nonlinear wave process (excluding the harmonics), which requires third-order nonlinearity in the system. We will not discuss here the weaker higher-order nonlinear effects, which also might contribute in the TBL physics.

In Sect. 3.2 we are discussing representative wavelet bispectra in Plates B5 and B6.

## 3 Sites of magnetosheath plasma penetration on 29 May 1996

In this section we discuss in detail the correlative measurements of Interball-1 and Polar at the magnetospheric boundary on 29 May 1996.

### 3.1 Wave signatures in the turbulent boundary layer

We start from an interesting feature between the MP and the rotational discontinuity (RD) see details in Savin et al., 1998a) in Plate A2(d): the kinetic energy density exceeds the thermal one. This means that the magnetosheath flow just outside magnetopause is supersonic (the sound Mach number $M_s \sim 2$, while the Alfvénic Mach number $M_A \sim 0.9$). This picture resembles the "Laval nozzle" or "wave" cusp model (see Yamauchi and Lundin, 1997). The model scheme is reproduced in Fig. 1. The thick curved arrow shows the inferred Interball-1 orbit. We would like to mention the general agreement between the model and measured velocities on panel (e). The measured $V_z$ demonstrates a negative wave train and then tailward acceleration at and just after the MP.
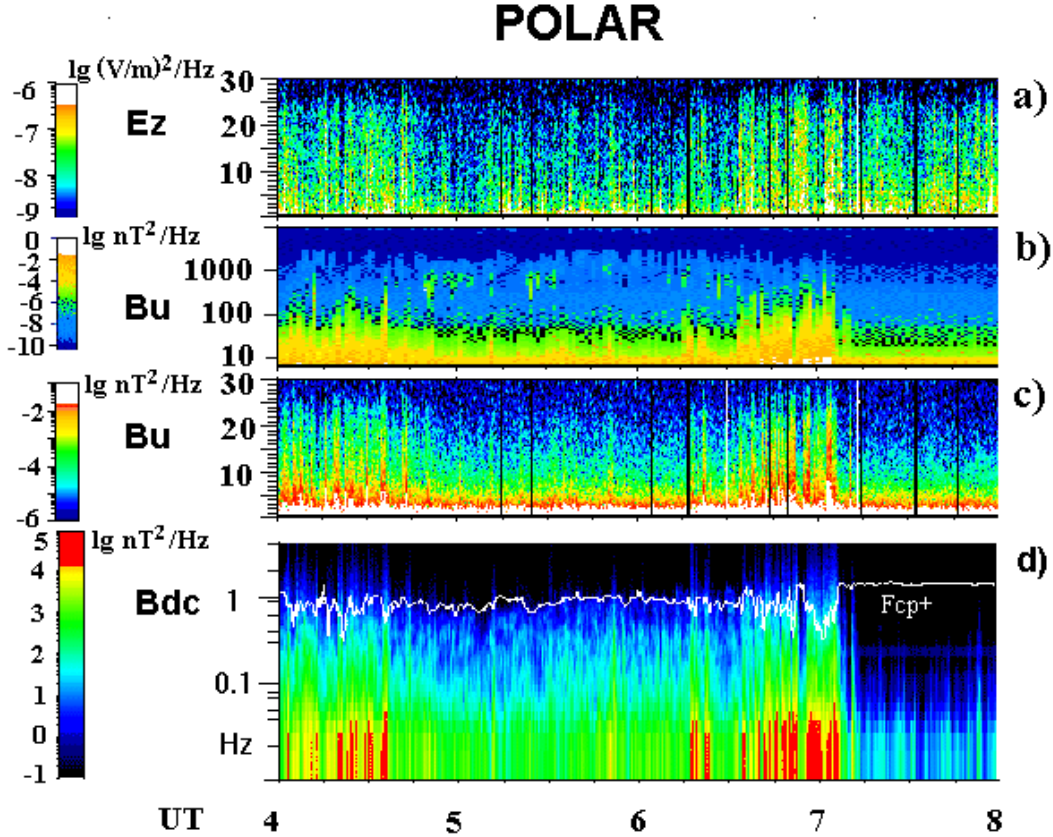
## POLAR



**Fig. 2.** Panels **(a)**, **(c)**: electric $E_z$ and magnetic ($B_u$) Fourier spectrograms in the spacecraft frame from the PWI instrument (note the linear frequency scale on the vertical axes for $E_z$ and low frequency $B_u$ (panel c) and the logarithmic scale on panel (b). Panel **(b)**: $B_u$ aboard spectra. Panel **(d)**: Fourier spectrogram of the total power of the DC magnetic field (sampling rate 8 Hz, MFE experiment); the white line depicts the proton cyclotron frequency labeled Fcp+.

$V_x$ is generally negative which corresponds to a streamline of MSH flow around the outside of the MP and inside the mantle. As it has been discussed in Savin et al. (1998a), the mantle existence during northward IMF is unusual and can imply MSH plasma penetration upstream of Interball, while the positive wave train in the measured $V_x$ prior to or at the MP clearly points to reconnection downtail and $V_z$ in the wave train agrees with the latter, too. We will return to the "Laval nozzle" model in Sect. 6.4.

Romanov (1998) and Savin et al. (1998b) have demonstrated that in the TBL the incompressible elliptically polarized waves are dominating at frequencies less than the proton gyrofrequency. However, unlike the linear Alfvén waves, the TBL contains "magnetic bubbles" with heated plasma and low total magnetic field inside. Wave power $Df$ in the TBL exceeds 30% of the ion energy density in the MSH, (Plates A2 and B1). An Interball "turbulent zone" encounter on the tail field lines has been presented by Klimov et al. (1997). The magnetic field spectrograms demonstrated a very clear TBL, while the electric field spectra also had rather high amplitudes just inside the MP. The same type of behaviour is observed in the Polar/PWI data near the dayside TBL on 29 May 1996 in Fig. 2. The spectrogram $E_z$ (panel a) demon-

strates spiky activity in the TBL at 04:00–04:45 and 06:17–07:08 UT, simultaneous with the ULF magnetic bursts seen in panels (b–d). In the polar cap at 07:55–08:10 UT there are electric field bursts, similar to those observed in the TBL, without corresponding ones in the magnetic field. The TBL magnetic bursts are quite wideband, reaching the electron cyclotron frequency (panel b). In between the TBL crossings and at their outer borders one can see spectral maxima from 200 to 1000 Hz, which correspond to the "lion roars", a characteristic feature of the MSH encounters (Anderson et al., 1982). The most prominent "lion roars" maxima are located near 300 Hz, which corresponds to the Magion-4/SAS data at 04:00 UT in the near-MP MSH (panel (h) in Plate A2). Magion-4, being at (4, −3.6, 8.7) $R_E$ in the GSM frame, is ~1500 km ahead of Interball-1 along the orbit track (cf. Blecki et al., 1998). Thus, the Polar/PWI data support the Polar encounter of the stagnant MSH on 29 May 1996 in between the TBL crossings. In the lowest frequency band the ULF waves have a maximum at 0.01–0.1 Hz, which agrees both with Savin et al. (1998b) for 21 and 2 April 1996 with IMF $B_z < 0$ (for the major part of the TBL) and with earlier reported characteristic plasma fluctuation periods from Heos-2 (Haerendel, 1978). A clear emission slightly below
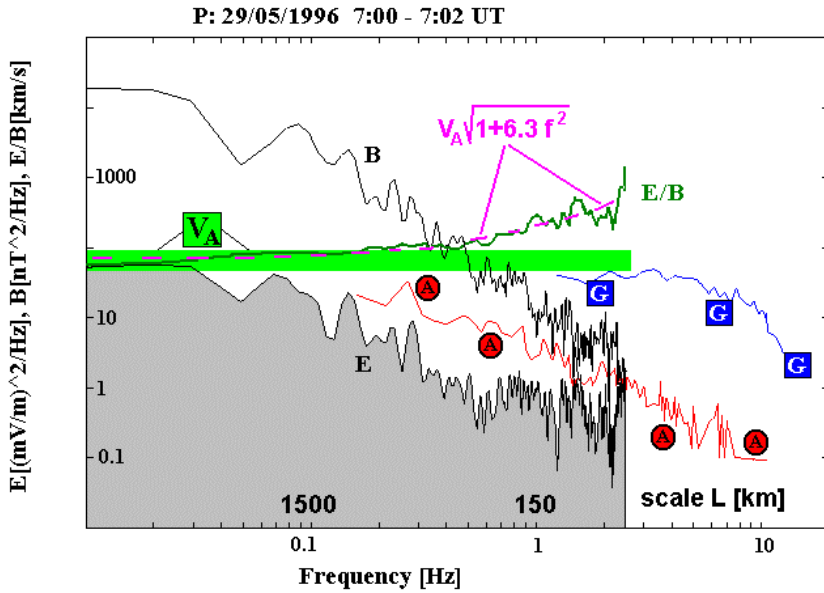
**Fig. 3a.** Electric ($E$, gray shadowed) and magnetic ($B$) Fourier spectra from Polar at 07:00–07:02 UT on 29 May 1996, $E/B$ – thin green line (in km/s); dashed line – KAW frequency dependence for $E/B$ from Eq. (5); Alfvén speed $V_A$ – thick green line. Squared 'G': Geotail electric spectra in TBL, 11:38–11:42 UT on 27 August 1995. Circled 'A': electric spectrum in cusp, Interball-2, 00:58 UT on 22 January 1997.
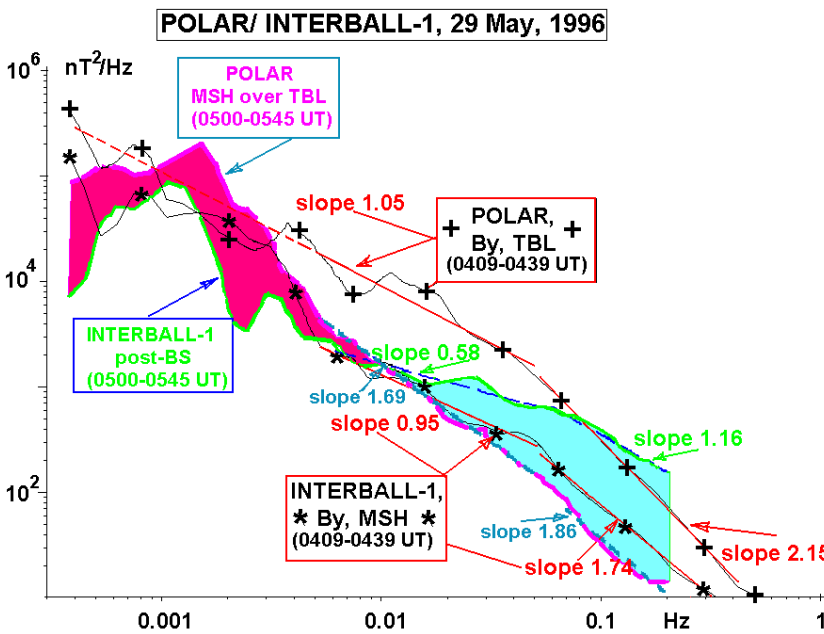


**Fig. 3b.** Magnetic wavelet spectra of GSM $B_y$ on 29 May 1996. Polar: TBL at 04:09–04:39 UT (crosses, the characteristic slopes are marked by the red color) and stagnant MSH over TBL at 05:00–05:45 UT (violet trace, slopes are marked by the blue color, the difference with the simultaneous post-BS spectrum from Interball-1 is shadowed). Interball-1: MSH at 04:09–04:39 UT (asterisks, the characteristic slopes are marked by the red color) and post bow shock MSH at 05:00–05:45 UT (green trace).

the He$^{++}$ cyclotron frequency is seen in Plate A2g at 02:56–03:04 UT. Weak emissions close to the proton cyclotron frequency, Fcp+, can be recognized at 03:05–03:13, 03:35 and 03:57 UT (cf. Klimov et al., 1986; Savin, 1994; Klimov et al., 1997). These ion cyclotron emissions outside the TBL indicate that non-equilibrium ion distributions are generated in the TBL (cf. Belova et al., 1991, Treumann et al., 1995).

To compare the ULF waves in the central TBL, near the boundary between the mantle and LLBL field lines and in the low altitude cusp we present the characteristic electric and magnetic Fourier spectra in Fig. 3a. The full upper curve displays the sum of the powers of 3 Polar magnetic field components (marked "B"), and the lower gray shadowed curve

shows the electric field components at 07:00–07:02 UT in the TBL (see Plate B3 for the survey). The electric to magnetic field amplitude ratio provides a proxy for phase velocity (marked by "$E/B$"). The Alfvén speed, $V_A$, is shown by the horizontal thick light line, with $E/B \sim V_A$ for the dominant waves in the TBL. We refer to them as Alfvénic Nonlinear Vortices. The magnetic vector hodographs in the minimum variance frame shown in Fig. 4 illustrate their vortical nature. The first vortex-like signal from Interball-1 in Fig. 4a corresponds to the $V_x$ and $V_z$ sunward wave train in Plate A2(e). For the planar geometry the wave vector direction is in the minimum variance direction, $B_k(0.64 - 0.72\,0.25)$. Avanov et al. (2001) calculated the de Hoffmann-Teller velocity

**INTERBALL-1, May 29, 1996, MIF-M**

03:17:05 - 03:17:45  UT
Ai =  363.59  ei = -0.0407  0.2977  0.9538
Aj =   88.95  ej =  0.7646  0.6238 -0.1621
Ak =   43.76  ek =  0.6433 -0.7227  0.2530
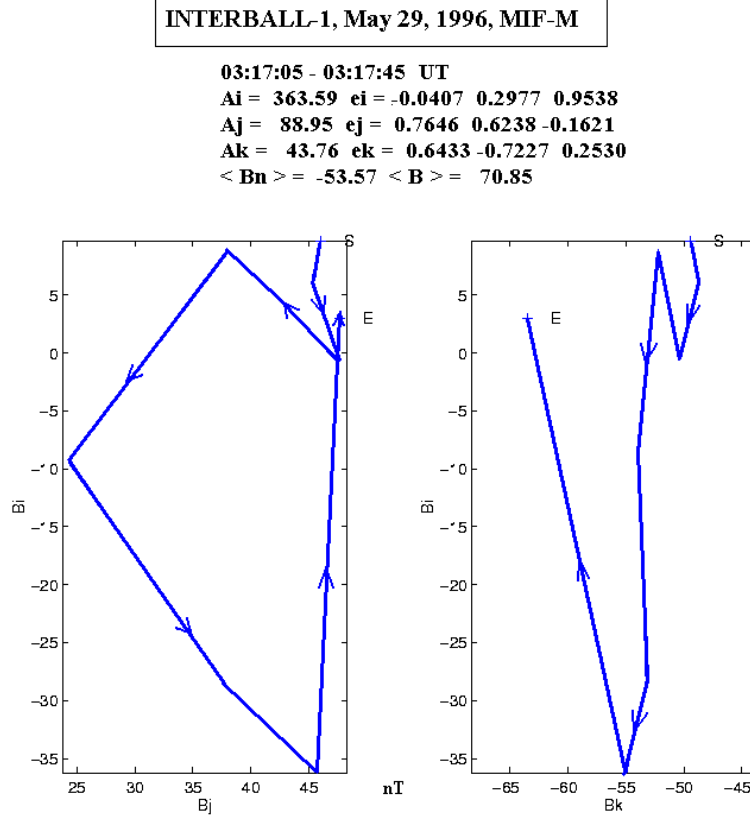< Bn > = -53.57  < B > =  70.85



**Fig. 4a.** Magnetic field hodogram of the Interball vortex-like structure in the main MP current sheet on 29 May 1996. The vortex scale in the minimum variance direction is estimated by ∼1000 km (see text for details). The maximum, medium and minimum variance eigen values and eigen vectors are given at the top of the figure in the GSM coordinate system along with the average normal component ⟨*Bn*⟩ and the magnetic field magnitude ⟨*B*⟩.

for the middle of the vortex interval of $V_{HT} = (32 - 178\,98)$ km/s. From this we estimate the vortex space scale $L \sim 2\pi/k$. For the Alfvén wave in the time domain, the frequency in the spacecraft frame is $f' = f + (k/2\pi * V_{HT})$. In the plasma frame it is $f \sim k\,V_A/2\pi$ (see Fig. 3a). We find for typical parameters, $L \sim 650$ or $1700$ km, depending on the $k$ sign. For pure spatial structure with $f = 0$, $L \sim 520$ km. Thus, one can accept $L \sim 1000$ km as a reasonable value for the vortex scale. It represents several tens of ion gyroradii for the measured plasma parameters.

Figure 4b shows an example of a magnetic field vortex-like structure from the Polar TBL inside the interval of the Polar spectra in Fig. 3a. Figure 4c displays the more irregular behaviour of the electric field at the same time. To check if the TBL waves in Fig. 3a can be regarded as spatial structures passing Polar, we approximate the $E/B$ ratio by the dispersion curve of the kinetic Alfvén waves (KAW). Near Polar apogee, Stasiewicz et al. (2001) have shown that the KAW with speed $V$ and ion gyroradius $\rho_i$ should result in $E/B$ in the frequency ($\omega$) domain in the satellite frame of reference as follows:

$$(E/B)^2 \sim V_A^2 \left(1 + (\rho_i\omega/V)^2\right). \qquad (5)$$

We present the calculated $E/B$ ratio from Eq. (5) by a

dashed line in Fig. 3a for $V_A \sim 70$ km/s, $\rho_i \sim 60$ km and $V \sim 150$ km/s (cf. Plate B1). The average measured $E/B$ ratio behaviour is close to that expected for KAW, while at frequencies over 1 Hz, high amplitude fluctuations around the average value are seen. These fluctuations correspond to the random ones observed on the electric field hodogram in Fig. 4c, i.e. most probably due to the electrostatic waves in the proton gyrofrequency vicinity. If our interpretation of the waves as KAW is true, we can roughly re-scale the $E$, $B$ and $E/B$ spectra in Fig. 3a into the space domain, as shown in Fig. 3a above the horizontal axis by $L$ (in km). Note that for the typical TBL frequency of 0.1 Hz, the inferred scale is close to that of Interball, namely to 1000–2000 km. Thus, different methods provide compatible scales for the vortex-like fluctuations in the TBL.

Returning to Fig. 3a we mark by the squared white "G" one of the strongest electric field spectrums in the TBL-like region, which has been detected aboard Geotail on 27 August 1995 during highly disturbed MSH conditions ($Df > (15\,\text{nT})^2$ at (4.5; 10.4; 4.2) $R_E$ in GSM frame; see also Fig. 8a for the position of this crossing marked by squared gray "G"). The electric field AC power for this disturbed case is more than one order higher in magnitude than that of Polar in the TBL on 29 May 1996. This fact indicates that in
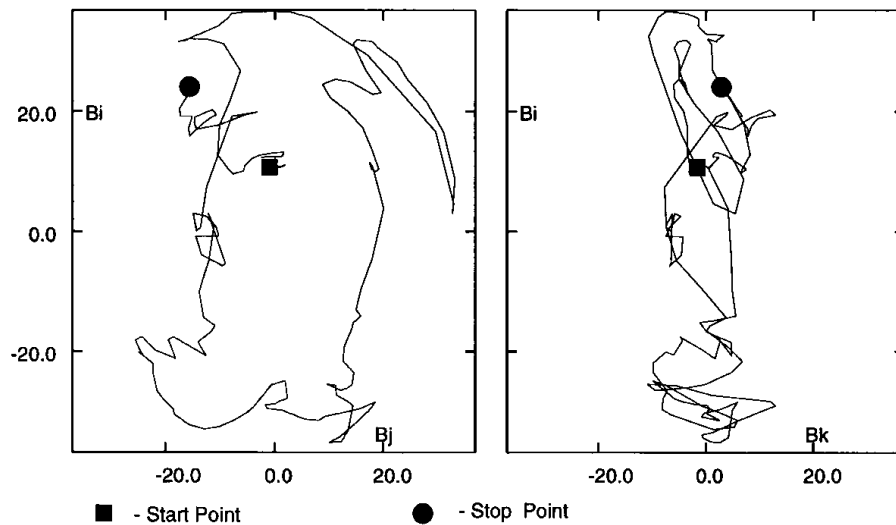
**Fig. 4b.** Magnetic field hodogram of the Polar vortex-like structure in the main MP current sheet on 29 May 1996 at 07:00:43–07:00:52 UT. The maximum, medium and minimum variance eigen values and eigen vectors in the SM coordinate system are: $Ai = 505.9, ei = (0.39; -0.46; 0.8); Aj = 204.4, ej = (0.14; -0.83; -.55); Ak = 28, ek = (0.91; 0.33; -0.26)$.
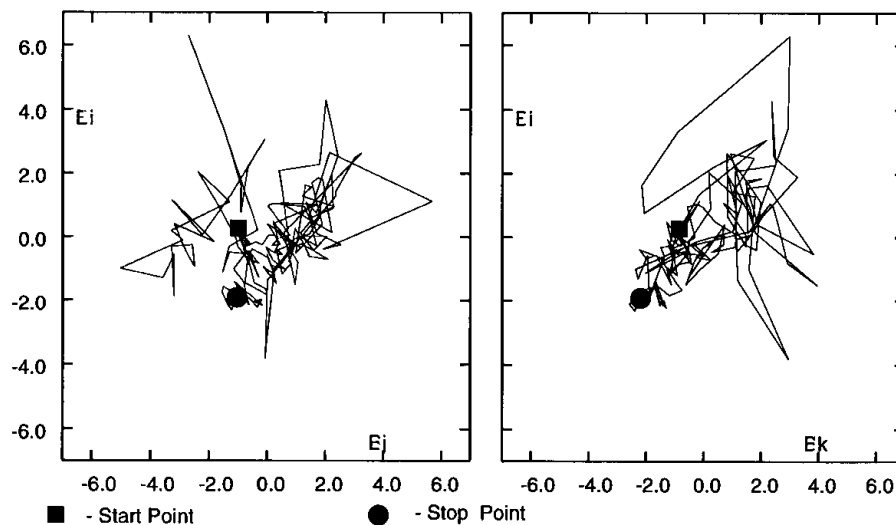


**Fig. 4c.** Electric field hodogram of the Polar vortex-like structure on 29 May 1996 (see Fig. 4b) in the same coordinate system as in Fig. 4b.

disturbed SW conditions the fluctuation power near the MP can be much higher than in the TBL on 29 May 1996, representing a case with highly compressed magnetosphere by the dense MSH (see Fig. 8). We suggest that the higher-level disturbances correspond to dynamic interactions of SW discontinuities with the MP.

Just inside the MP the magnetic wave power drops sharply (see Plates A2(f, g) and B1(f)), so that the waves can hardly heat the core proton and alpha particles by their own energy. Instead, they are a good indicator of the plasma non-equilibrium state and represent the mean for the energy redistribution between the particle species and for diffusion in velocity space. The Polar case of the thick MP at about 04:00 UT is an exception: at 03:38–04:08 UT the $Df$ is

higher than usual (cf. Savin et al., 1998b, and Plate B1(f) and Fig. 2 at ~07:10 UT). Interball-1 data also display the enhanced wave power at 03:00–03:15 UT, where the quasi-perpendicular, reflected and "fresh" injected ions are mixed and the strong waves are generated in such extremely non-equilibrium plasma (see Plate A2). In the deeper weak cusp and mantle at 02:00–02:55 UT only weak magnetic spikes are seen, mainly indicating plasma flow gradients (panel f).

At the lower altitudes in steady situations only electric field variations are usually seen. A characteristic example for the low altitude cusp variations from Interball-2 was observed on 22 January 1997 and is shown in Fig. 3a by the curve marked by a circled "A" (at 00:58 UT at a height of 2.3 $R_E$). While its absolute power exceeds that of the Po-
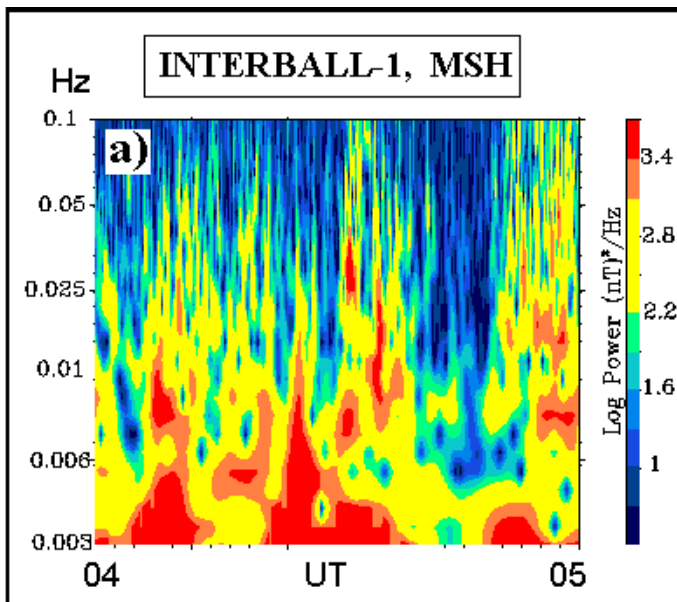
**Fig. 5a.** Interball-1 wavelet spectrogram in the MSH ($B_y$ GSM component, 0.003–0.1 Hz) at 04:00–05:00 UT (see also Plate A1);
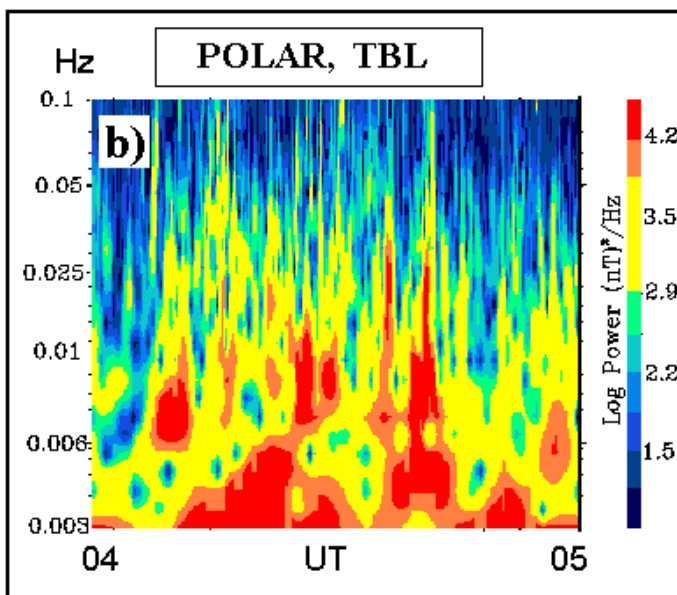


**Fig. 5b.** The same for Polar in the TBL (see also Plate B1).

lar TBL (gray shadowed), the scaling factor in the divergent Earth's magnetic field reduces the low altitude equivalent power to more than an order of magnitude less at the Polar apogee height. During geomagnetic disturbed conditions Pickett et al. (1999) also reported the specific ULF wave activities in the low altitude cusp in conjunction with the energetic particle bursts. Unlike the TBL, the magnetic fluctuation power deep in the cusp is negligible as compared with the local DC magnetic field pressure.

Now we would like to make use of the simultaneous Interball and Polar magnetic field measurements in different regions near the MP. A poorly explored problem is how the MSH-born fluctuations influence the TBL turbulence. We present wavelet spectrograms (see Sect. 2.3) of the GSM $B_y$ components from the MSH (Interball) and TBL (Polar) at 04:00–05:00 UT in Figs. 5a and b. Note clearly outlined wave trains (i.e. isolated maxima) at different frequencies simultaneously that indicates the presence of multi-scale nonlinear processes. The linkage between the maxima represents a feature of cascade processes, where the direct/inverse (i.e. high or low frequency fluctuations appear first) cascades might be inferred. While the spectral character in the MSH and TBL seems to be similar, no detailed correlation is seen, especially for the frequencies >0.03 Hz and at 04:50–05:00 UT. Note also the color scale difference: the TBL spectra are of about an order of magnitude more in-

tense. We have found that the general correlation of the $B_y$ components on Polar (in the TBL and stagnant MSH) and Interball (in the nominal MSH) on the time intervals of 0.5–1 h is poor (<0.2), while for disturbances such as MSH discontinuities the correlation can reach 0.7 on intervals of the order of 5–10 min. No well-defined time delays can be found (i.e. correlation functions are flat on intervals of several tens of seconds). The only disturbance on Polar at 05:26–05:45 UT having a respective counterpart in the Interball post shock data (not shown) has a correlation coefficient of 0.6 and the clear time delay of 925 s.

For quantitative comparison of the wave spectral features we present the characteristic integrated wavelet spectra (see Sect. 2.3) in Fig. 3b. We have chosen two intervals with Interball-1 as an upstream monitor in the nominal streaming MSH and Polar in or just over the TBL: (1) 04:09–04:39 UT with similar character of the wavelet spectrogram (Figs. 5a and b) and (2) 05:00–05:45 UT with Polar just outside the TBL (or even at its border, see Plate B1(f) and Fig. 2) and Interball-1 in the disturbed MSH just downstream of the bow shock (BS, see Savin et al., 1998a). Comparison of the magnetic spectral shapes in the TBL and stagnant MSH over the TBL versus the nominal flowing MSH from simultaneous Polar and Interball-1 data shows that the low frequency disturbances (at 0.001–0.002 Hz) can be transmitted throughout the MSH from downstream of the BS. This is seen from both the coincidence of the MSH and TBL spectral powers (asterisks and crosses) and the existence of the spectral peak at these frequencies throughout the MSH in two other spectra. The mechanism of the power amplification at these frequencies over the TBL is unclear (see dark shading of the power difference in Fig. 3b). There are several opportunities for this:

(a) amplification at the discontinuity (shock?) between the stagnant and flowing MSH;

(b) amplification due to convergence of the outer cusp throat;

(c) accumulation of the permanently inflowing disturbances in the stagnant OT;

(d) out-flowing of the waves from the TBL (note the higher frequency of the peak near 0.001 Hz on Polar at 05:00–05:45 UT in Fig. 3b). As for the disturbances at frequencies >0.01 Hz, they appear to dissipate downstream of the bow shock as their power near the MP is lower than near the BS (the respective difference is shaded light-blue).

The most characteristic TBL waves at 0.005–0.5 Hz happen to have the characteristic kinked spectral shape and slopes (note the higher power and different shape in this frequency band of the spectrum marked by crosses in Fig. 3b). In the TBL this expectation of the intermittent quasi-coherent structures is realized in Alfvénic nonlinear vortices (ANV), which are displayed in Fig. 4 (see discussion above). The spectral power here is much higher than that of fluctuations

in the flowing and stagnant MSH, and the spectral shape is different: the kinked shape with the slopes of 1–1.5 and 2–2.6 are those characteristic of the TBL, while a spectral peak at lower frequencies might also appear (cf. the dark-shaded spectrum over the TBL in Fig. 3b). A substantial TBL feature, which coincides (we suppose by chance, see discussion in Sect. 6.5 below) simultaneously with the one in the MSH shown in Fig. 3b, is the frequency of the kink (asterisks and crosses).

To verify the local TBL origin of the turbulence, at least partially, we study Poynting flux on the interval of the Polar data in Fig. 3a (07:00–07:02 UT). In Plate B2 we present the Poynting flux angular distribution; its relative magnitude is shown by contours with incremental value of a factor of 2. The blue shading corresponds to the maximum Poynting flux magnitude. The GSM axes are labeled in circles; the $Z$ ($-Z$) axis corresponds to the upper (bottom) horizontal line. Crosses mark the direction of the average magnetic field, and the median frequencies of the intensity maxima are given in mHz. Note that the characteristic maxima have frequencies of 50–60 mHz, which corresponds to the most prominent maxima in the power spectra in Fig. 3a. Spectral analysis of the Poynting vector and its decomposition on the differently propagated waves has been performed using the method of Romanov (1998). In the interval under study negligible Poynting flux has positive projection on the average magnetic field (that is under the curve, showing the perpendicular plane to the magnetic field in Plate B2). Instead, the maximum electromagnetic energy is flowing both antiparallel to the magnetic field (close to the inclined blue cross) and nearly along the MP downstream of the cusp (i.e. $\sim$ in the middle between the $-X$, $Y$ and $Z$ axes). The fluctuation power has a characteristic magnitude for the TBL (see Plate B1(f) and Fig. 2). So, we conclude that a process poleward of Polar has comparable power with the processes at the origin of sunward jets at 06:45–07:00 UT (see Plate B1(b), Fig. 6 and related discussions below). This process, probably small-scale reconnection at the cusp-MSH interface, is certainly the inherent TBL one, i.e. the high level electromagnetic energy cannot originate from the remote reconnection site (see RRS in Plate A3 and A4 and related discussions below) at 07:00–07:02 UT, on the time interval of Fig. 3a and Plate B2.

Thus, we conclude that for the case under study substantial disturbances are generated in the TBL, having a character different from the waves in both the near-Earth MSH and the downstream bow shock. This inherent interaction is thought to be modulated by the MSH flow disturbances and discontinuities.

### 3.2 Turbulent boundary layer: random or organized?

Now we address the question of whether the sunward flows, MP-like current sheets and "diamagnetic bubbles" in Plates A2 and B1 are driven by random SW/MSH disturbances or whether they are the result of some kind of correlated or coherent behaviour, at least during rather stationary SW pe-
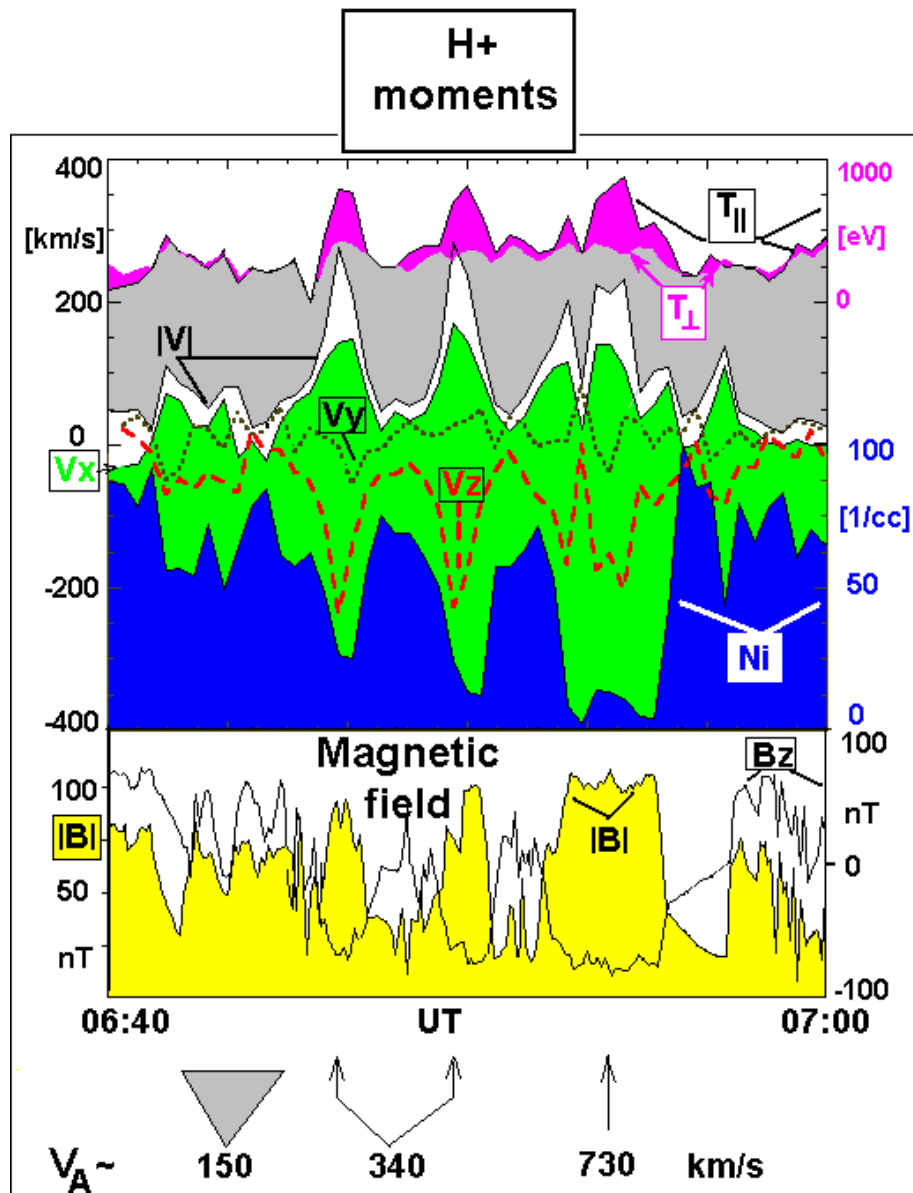
**Fig. 6.** Coherent structure in the inbound TBL from Polar (see Plates B1, B3, B5). Top panel: TIMAS proton moments – temperature (violet shading depicts the difference between the parallel and perpendicular temperatures), velocity ($V_x$ – green shading, $V_y$ – dots, $V_z$ – red dashed line) and density (blue shading). Bottom panel: magnetic field $B_z$ (the scale at the right) and $|\boldsymbol{B}|$ (yellow shading, the scale at the left). Bottom line: Alfvén velocity in the MSH (gray triangle) and inside high-speed jets (arrows).

riods. In other words: can the local TBL processes (including reconnection-like) be regarded as a collective multi-scale interaction pattern? In Fig. 3b we have already demonstrated a feature compatible with a self-organized process, namely power-law kinked spectra in the TBL (curve marked by crosses) but, for example, the streaming MSH could have spectra of similar shape (curve marked by asterisks). To obtain further insight into the problem we show in detail Polar parameters in the inbound TBL crossing (Fig. 6) and analyze the $B_z$ component by the Morlet wavelet transform, wavelet correlation time and bicoherence (Plate B3–B5 see also Sect. 2.3).

In Fig. 6 we show high time resolution TIMAS mass-spectrometer proton moments and magnetic field in the TBL at 06:40–07:00 UT: the parallel (upper black line) and perpendicular (violet line) temperatures (linear scale at the right side, the difference between the parallel and perpendicular temperatures is indicated by the violet color), the ion velocity $|\boldsymbol{V}|$ (upper gray shading), GSM $V_y$ and $V_z$ (dotted black and dashed red lines), $V_x$ (lower green shading) and the density $N_i$ (lower blue shading, linear scale at the right side). At the bottom of Fig. 6: characteristic Alfvén speed, $V_A$, in the disturbed MSH (gray shading) and in the velocity jets (marked by arrows). The bottom panel displays GSM $B_z$

(linear scale at the right side) and $|\boldsymbol{B}|$ (yellow shaded). $B_z$ is generally positive in the MSH and negative in the lobes (cf. Plate B1(a)). Velocity sunward jets (up to $|\boldsymbol{V}| = 285$ km/s) are pointed in a counter-streaming direction (i.e. $V_x > 0$, $V_z < 0$). They clearly correlate with the minima in $N_i$ and negative (magnetospheric-like) $B_z$. Another characteristic jet feature is parallel heating. Note also the general excess of the parallel temperature in the region of jets and "bubbles" at 06:45–06:57 UT: this strongly suggests that mirror waves cannot account for the "diamagnetic bubbles" formation, because for the mirror instability, the perpendicular temperature should exceed the parallel one (see, e.g. Stasiewicz et al., 2001 and references therein). Angles between the magnetic field and three velocity jets, marked by arrows at the bottom, are, respectively, 16.5, 16.5 and 29 degrees (from left to right). Thus, the jets are practically field-aligned, being accelerated to velocities between the local and MSH Alfvén speeds. The presence of these jets, along with the "diamagnetic bubbles" and parallel proton heating, strongly infers field-line reconnection downtail of the Polar position. The dynamic pressure in the jets (i.e. $2E_{kin}$, see Plate B1(d)) is of the order of the $Em$ around the jets that also conforms to the jet acceleration by transformation of the magnetic energy in magnetic field reconnection. The density $N_i$ anticorrelates with $|\boldsymbol{B}|$. This might be regarded as random MP crossings. On the other hand, the velocity wave train in Fig. 6 is rather regular and remarkably resembles that of Interball in Plate A2(e). One possibility is that both of them result from the downtail RRS, while for Polar it is not reproduced by the global MHD model (see Plates A2, A4, B1). In this case the reason for the patchy character of the reconnection might be in the high flow velocity near RRS (with nearly Alfvénic and at some times supersonic velocity, see Plate A2 and discussions above), which prevents the occurrence of stationary reconnection (see La Belle-Hamer et al., 1995).

We would also like to discuss another data explanation that suggests, for example, local TBL reconnection, Alfvén resonator, etc. (cf. Savin et al., 1998a, 2002b; Stasiewicz et al., 2001). In Plates B3–B5 we present the results of detailed wavelet analysis for the chosen TBL interval. Plate B3 shows a wavelet spectrogram for 0.00156–0.05 Hz. It is similar to that of Fig. 5b: the isolated maxima correspond to wave trains; they constitute the cascade-like chains that are tentatively shown by black curves with respective circled numbers. The inverse (1, 3) and direct (2, 4, 5) cascades could be inferred, with the most prominent ones being marked by the numbers 2 and 5. The main wave train, visible in Plate B1(b) and Fig. 6 throughout the TBL at 06:40–07:10 UT, corresponds to the long stable maximum at $\sim$3.3 mHz in the Plate B3. The maximum at 1.6–1.7 mHz is visible even inside the magnetosphere. We have checked that the $V_z$ and $V_x$ spectrograms have a similar character to that of $B_z$ in Plate B3, while for different components the different maxima are most explicit.

In Plate B4 we present wavelet correlation time (see Sect. 2.3) in the range of 2.5–80 mHz for the TBL and MSH crossing by Polar; Insert A displays that of the Interball-1

outbound MP/TBL crossing for comparison. The TBL crossing on Polar is specified by the highly coherent (correlation time >3 periods) wave trains, visible at the low frequencies for several sub-intervals of the analysis. The most prominent feature in the Polar TBL is a coherent structure at $\sim$07:00 UT (marked by an ellipse with the circled label A); this is namely the wave train at $\sim$3.3 mHz outlined in the discussion of Fig. 6 and Plate B3. The higher frequency coherent signals (e.g. at 17, 23, 35, mHz, cf. Plate B3) are not specific only to the TBL. The inbound TBL at $\sim$04:30 UT is also characterized by coherent wave trains but at several frequencies simultaneously ($\sim$2.8, 4.5, 6.7 and 8.5 mHz, cf. Fig. 5b). These coherent wave trains are hardly obvious from the waveforms or Fourier spectra in Fig. 2c–d at $\sim$04:30 UT (we checked that the corresponding maxima are seen in the $V_x$ and $V_z$ wavelet spectrograms as well). While the period of $\sim$3 mHz signal on Interball (Insert A) is short (of the order of the TBL crossing time, see Plate A2), the wavelet analysis demonstrates a greater correlation time at this frequency (>2 periods) than at the neighboring frequencies. This is rather interesting as Interball and Polar crossed the outbound/inbound TBL at about the same $X$ and $Z$ (see Plate A3), while at different times and at symmetric $Y$ relative to noon. The difference in the duration of the TBL encounters is, most probably, due to the Interball crossing of the current sheet $\sim$ along the normal, while the orbit of Polar is nearly elongated along the MP current sheet (see Plates A3–A5). The coherent Interball signals throughout the MP/TBL crossing are visible at $\sim$5 and 18 mHz; the 5 mHz one corresponds to the well visible $V_x/V_z$ wave train in the Plate A2(e). Thus, in both cases the coherent magnetic and velocity signals are seen for a long time throughout the cusp/MSH transition. This is different from both the usual concepts of stationary reconnection and random reconnection bursts: in the former case the repetitive flows should not be seen during $\sim$ steady solar wind conditions; in the latter case the bursts should be random instead of coherent.

In Plate B5 we present the bicoherence spectrogram (see Sect. 2.3) for $B_z$ SM in the Polar inbound TBL on 29 May 1996, 06:40–07:10 UT, i.e. from nearly the same core TBL intervals as the spectra in Plate B3. The frequency plane ($f_k$, $f_l$) is limited by the signal symmetry considerations and by the frequency interval of the most characteristic TBL slope of $\sim$1 in Fig. 3b. As we mentioned in the Sect. 2.3, the bicoherence in the TBL displays the second and higher harmonic nonlinear generations and, most probably, three-wave processes, with cascade-like features that are visible at the vertical axis $f_l \sim 0.003$ Hz (i.e. at the coherent wave train labeled by "A" in the ellipse in Plate B4). We assume cascade signatures in Plate B5, when the bicoherence at the sum frequency, $f = f_1 + f_k$, has a comparable value with that of point ($f_k$, $f_l$). In the case of the horizontally-spread maximum, it is implied that the wave at sum frequency interacts with the same wave at the initial frequency ($f_A$ in our case) in the following three-wave process: $f3 = f_A + f_k$, etc.; the initial wave spectrum can be smooth resulting in the continuous bi-spectral maximum. Most characteristic frequencies,

which one can see in Plates B3 and B4 (e.g. $f_1 \sim 4.5$, 6.7, 18, 23, 36 mHz), are also proved to participate in the multi-wave coherent processes that give maxima in Plate B5. For example, the following processes could be inferred: horizontal cascade $f_l \sim f_A + 23 = 26.3$ mHz, $f_A + 26.3 = 29.6$, etc. until $\sim 100$ mHz; $4.5 + 18 \sim 23$; cascade $6.7 + 23 = 29.7$, $6.7 + 29.7 = 36.4$, $6.7 + 36.4 = 43.1$ mHz. Another set of nonlinear processes is realized with the harmonic generations and their further interactions: on the spectrogram diagonal 3 the strongest maxima are close to the first, with second and fourth harmonics of the "resonant" frequency $f_A$; the respective processes are labeled in the figure, including the third harmonic generation. Further, multi-wave interactions of the harmonics could be inferred as well: $1.5 + 2f_A$ (labeled at the bottom); cascade $2f_A + f$, etc., $4f_A + f$. Note from the Plate B3, that the 1.6 mHz signal penetrates the magnetosphere. Both 3 and 1.5 mHz maxima are also present in the Interball bi-spectra near the MP (not shown). While the process identifications are not unique (e.g. the four-wave modulation instability might be involved etc.) we certainly encounter a very complex picture of furcated multi-frequency (i.e. multi-scale) coherent interactions, which strongly indicate the presence of cascade processes, based on the "resonant" frequency $f_A$, seen in plasma parameters in Fig. 6 as well. As for the wavelet analysis of plasma moments, we should note that the number of points in the TBL is too small for the wavelet correlation time and bicoherence determinations, while wavelet spectrograms look quite similar to those of the magnetic field.

Inspection of the bicoherence spectrogram for the Polar outbound TBL in Plate B6 ($B_z$ SM component, 04:14–04:44 UT, the format is the same as for Plate B5) confirms the complex coherent picture of the TBL interactions. The respective frequency of the main cascade is close to the lowest one in Plate B4 at $\sim 04:30$ UT, i.e. $f_B \sim 2.6$ mHz, while the $2 f_B$-signal is weaker. Similar to Plate B4, the outbound bi-spectrogram displays coherent processes at several frequencies: the low frequency cascade (horizontally interconnected maxima) starts at $f_l \sim f_B$ (vertical axis), then at $f_k \sim 30$ mHz (horizontal axis) shifts to $f_l \sim 4.5$ mHz and for $f_k > 70$ mHz both cascades at $f_B$ and 4.5 mHz co-exist. Note that 4.5 mHz is close to the second from the bottom maximum at 04:30 UT in Plate B4; the next coherent process with maximum at $\sim 7$ mHz in Plate B4 probably contributes a lot to the most prominent maximum in Plate B6, labeled "$4 f_B + 4 f_B \sim 8 f_B$". The process "$f_B + 7$ mHz" has also a highly visible maximum on the bi-spectrogram along with the second harmonic nonlinear generation: $7 + 7 = 14$ mHz. This second harmonic in turn looks to interact: $14 + 35 = 49$ mHz. The lower frequency bi-spectra in Plate B5 also reveal strong nonlinear interactions at $\sim 1.5$ mHz, i.e. close to that in Plate B3, which penetrates inside the MP (see discussion of Plate B3 above). Despite the differences in Plates B4 and B5 the main cascade-like nonlinear interactions look very similar on both, i.e. the main cascade is synchronized by low ("resonant") frequencies throughout the wide frequency band.

Thus, the results of the modern wavelet data analysis technique strongly indicate that the TBL fluctuations are highly coherent, multi-scale and "organized" in cascades of nonlinear interactions. The chosen coherent wave trains appear to synchronize the interactions throughout the TBL, i.e. a kind of over-TBL resonance.

We return now to the detailed comparison of the experimental and model data (see also Sect. 2.2).

## 4 Comparison with MHD model

Intersection of the Polar orbit with the model boundary in Plate A4, labeled by the dashed black-and-white line (marked "$n > 401/cc$"), agrees with the outer cusp encounter by Polar at $\sim 03:20$ UT, as it is seen from the rise of the model $V_x$ ($V_z$) and that of $Df$ in Plate B1(c, f). Polar returns inside the MP at 07:08 UT, which is reproduced by the MHD model with about a 10 min delay. The delay is seen by comparing the $V_x/V_z$ vanishing at the right part of Plate B1(c) with the final $B_z$ transition to the negative value in Plate B1(a). This delay seems to be characteristic for the total reproduced interval (see, e.g. the model $V_x$ sign changes at $\sim 04:20$ and 05:20 UT relative to the measured $V_x$ ones). The measured magnetic field displays a substantial discrepancy at the inbound MP (see Fig. 6 in Russell et al., 1998) due to an inability of the model to reproduce sharp gradients ($< 1000$ km). The model velocity generally agrees with that of the measured one up to $\sim 06:30$ UT, including the sunward ion flow in the cusp and outbound TBL (Plate B1(b)). In the stagnant MSH decelerated flow still continues to move downtail ($V_x < 0$, $V_z > 0$). The impulsive flows at 04:00–04:40 UT look to be of local origin, having unpredicted high velocities and strong $V_y$ components: at 04:02 UT $V = (28\,105 - 73)$ km/s with the $|V| = 131$ km/s, i.e. close to $V_A$ in the MSH, the model $V_m = (32 - 16 - 24)$ km/s; at 04:08 UT $V = (80\,68 - 89)$ km/s with $|V| = 138$ km/s, i.e. again close to the $V_A$ in the MSH, the model $V_m = (32 - 11 - 19)$ km/s; and finally at 04:36 UT $V = (100\,50 - 71)$ km/s with $|V| = 133$ km/s, the model $V_m = (4 - 39 - 30)$ km/s. We have already discussed above the measured wave trains at 06:40–07:10 UT. Note also the anti-correlation of the spikes in $Em$ and $E_{kin}$ in the TBL (Plate B1 d). Here we would like to remind the reader that, while the wavy-velocity jets aren't reproduced by the model, they still might originate from the RRS. However, we assume a generally local origin of the main TBL fluctuations (see previous section). Indeed, in Plate A4 the thick intensive current sheet (red-colored) spreads from the sunward wall of the outer cusp throat to the RRS, i.e. the model infers a stretched-out disturbed zone. We cannot check that from the spacecraft data on 29 May 1996 but the model indicates the probable TBL spread from the RRS to the sunward OT wall (i.e. $\sim 04:30$ UT in Plates B1 and B4).

As for Interball-1, note the positive/negative model $V_x/V_z$ velocity drift just prior to the MP in Plate A2(e); the model reproduces the average tendency of the measured speed, but not its fine structure (i.e. the wave train). The most proba-
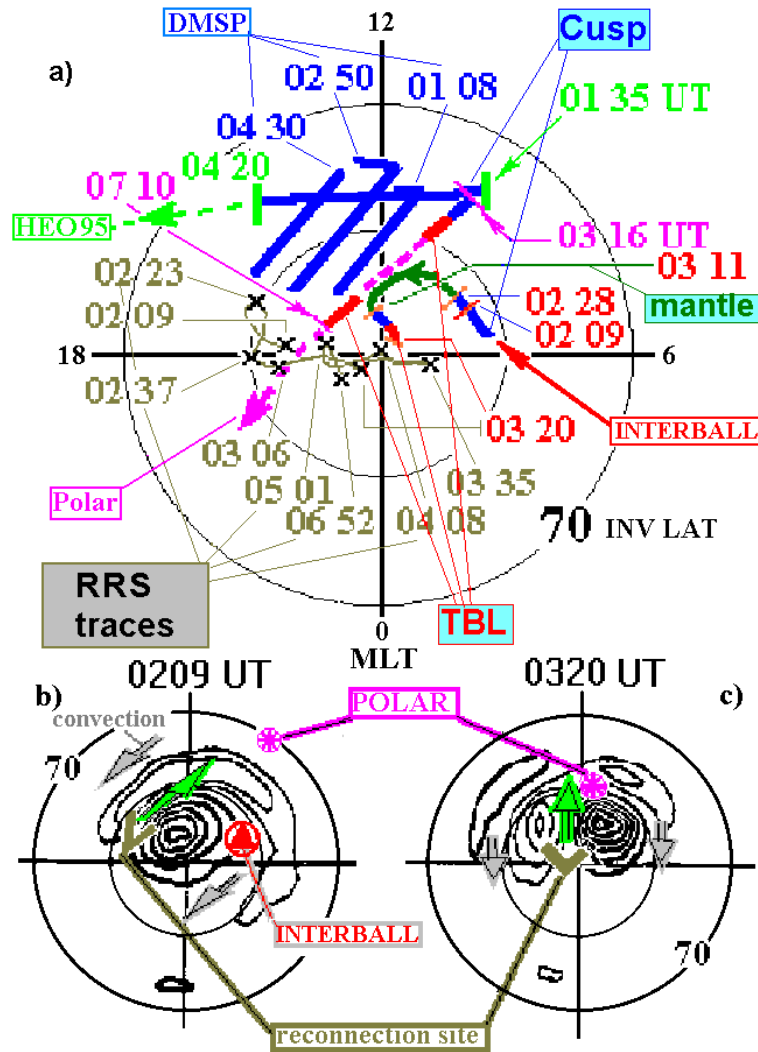
**Fig. 7.** Projection onto the northern ionosphere in (Invariant Latitude/ MLT) coordinates on 29 May 1996. **(a)** Cusp (blue), mantle (green), TBL (red) ionospheric traces for different UT and spacecraft, marked in the figure and the traces of remote reconnection sites (RRS) for different UT from the global MHD model (inclined crosses) **(b)** ionospheric equipotential contours for a cross-cap potential of 6 kV and field-aligned current of $4\,10^{-6}$ A/m. at 02:09 UT from the global MHD model and **(c)** the same for 03:20 UT. Traces of Polar (violet asterisks), Interball-1 (red circled triangle) and reconnection point footprints (RRS, brown arrows) are depicted along with the convection directions (along the contours, green arrows in the center and gray ones at the periphery).

ble reason for that is the rather crude model grid ($>0.2\,R_E$, see details in Fedder et al., 1995), while the influence of the local medium-scale disturbances, reproduced by the model, on the global structure is not excluded (see discussions in Sect. 2.2). One can see a systematic difference in the measured and model $V_x$ between the MP and 03:30 UT; after that time $V_x$ fits the model well. Detailed study of high-resolution ion data by Avanov et al. (2001) provides further proof for the registration of the features predicted by the model reconnection site being downtail of Interball (Alfvénic field-aligned flows in the de Hofmann-Teller frame, stress balance fulfilling, etc.).

Now we would like to address the problem of the mechanism for the MSH plasma penetration into the cusp (see

Fig. 7 and related discussion in Sect. 2.2). We assume that we have shown and sited enough experimental evidence for the RRS operation being in satisfactory agreement with the MHD model predictions. Let us consider three ways of the cusp populating by the RRS:

– filling while RRS merging is ongoing ("merging filling");

– convection inside the MP of the filled, by merging lines (closed) after merging termination ("convection filling");

– filling through the interconnected RRS lines after merging termination ("interconnection filling").

To estimate the trace range of "merging filling" we take the maximum convection distance for the cusp ions with the measured characteristic energy $\sim$500 eV, injected parallel to the magnetic field at the RRS. For 2 km/s as the reasonable limit of ionospheric convection, one obtains the trace drift $\sim$200 km (projected on the ionosphere) during time-of-flight of parallel 500 eV ions from the RRS to the ionosphere. The drift ionospheric velocity of 2 km fits the measured average positive $V_x < 50$ km/s in Plate B1(b) at 04:00–04:30 UT taking into account the scaling factor from the MP to ionosphere. The tracks of ions, traveling back towards the MP, will be shifted $\sim$400 km. The isotropic cusp ions at 01:30–02:20 UT (Plate A2 a) are seen at $\sim$2500 km from the RRS trace, i.e. more than 5 times larger than the drift path of reflected ions. This is best seen in Fig. 7b: the RRS proves to drive the two-cell sunward (see green arrow in the center) convection with the strong downward component due to large IMF $B_y$. Returning to the plasma reaching the ionosphere from the RRS while merging lasts, one can see that the plasma from the RRS cannot account for the Interball-1 cusp at 01:30–02:20 UT: the Interball trace is too far away. Obviously, the same is true for the HEO95-034 and most of the DMSP cusp periods.

In Figs. 7b and c one can see that reconnection drives the ionospheric convection (see the arrows); the contours display a permanent direction of the ionospheric flows upstream of the reconnection site projections throughout several hundreds of km. We suppose that this results from the narrowness of the RRS flows at its location; the flow direction corresponds to the antiparallel magnetic fields inside and outside the magnetosphere. The latter infers that the kinked reconnected lines are transported towards the dayside border of the cusp (after merging termination) in a rather narrow angle range. After the second reconnection in the Southern Hemisphere such an over-draped line could become a part of the low latitude boundary layer (LLBL, see Onsager et al., 2001 and references therein). Our expectation for the narrow reconnected flows is supported by the fact that in Plate B1(a, b) outside the MP, i.e. during positive $B_z$, generally $V_x < 0$ (both the measured and model). Thus, the majority of the MSH field lines in the decelerated OT moves tailward. Only two thin jets with $V_x > 0$, $V_z < 0$ (i.e. probable flows from RRS) are seen at 05:10 and 06:18 UT in the measured velocity during stable $B_z > 0$ in the MSH; the first has a counterpart in the model at 05:20 UT (with the above mentioned 10-min shift). We infer from that the narrowness of the sunward RRS flows as compared with the OT width: Polar traced the OT through more than $2 R_E$ in $X$ and almost $3 R_E$ in GSM $Y$ directions (see Fig. 8a), i.e. comparable with the average dimensions of the OT (Savin et al., 1998b). Looking now at Fig. 7 we would like to conclude that "interconnection filling" in the narrow angle range ($\sim$ in the green arrow directions) might account for the cusp on HEO at early dawn and at the noon trace part on DMSP at 01:08 UT, and at low latitude at 02:50 and a small portion of the trace at 04:30 UT. We will discuss the interconnected line filling in Sect. 6.2.

As for the "convection filling", comparison of Figs. 7a and b, Fig. 7c shows that: (a) only $\sim$ half of the DMSP cusps at high latitudes could be accounted for by the convection, (b) the Interball cusp at $\sim$02:09 UT lies on the respective convection line but the convection time is $\sim$1 h, which seems to be too long (cf. variability of RRS traces in Fig. 7a), (c) the Polar cusp can originate from the "convection filling", (d) the HEO cusp is inconsistent with it.

We would like to conclude that the dusk cusp on HEO, the low latitude DMSP cusp at 04:30 UT adjacent to HEO, and most probably the Interball cusp at $\sim$02:00 UT cannot be accounted for "by using" the three processes compatible with the MHD model. The wideness and stability of the cusp versus quite changeable RRS trace positions in Fig. 7a also confirm this (cf. Savin et al., 1998a). So, the combined model and in situ data support the suggestion that the RRS cannot be the only major source for the all cusp-like plasma that was registered on that day.

## 5   The case on 29 May 1996 on the background of turbulent boundary crossings in 1995–1998

We would like to relate the described case to the TBL crossings by Interball-1 in 1995–1998. The Interball-1 orbit evolution provided an opportunity to cross the near-cusp MP for most of a year, excluding the late October – late December time period, when the orbit apogee has been in the tail lobes. For this study we use the routinely calculated dispersion of $B_x$ raw magnetic field waveform with sampling rate 4 Hz at the 20-s intervals (i.e. for 0.05–2 Hz). To compare with $Df$ in Plates A2 and B1 in a statistical sense, we multiply the $B_x$ power variance by a factor of 3, suggesting the equality of the ULF power at all 3 magnetic components on average, that have been checked to be satisfactorily valid for 10 characteristic TBL crossings. We give the AC magnetic pressure ($= Df = $RMS$^2$) in [eV/cc] for comparison. For the TBL we have chosen a threshold of the maximum root mean square RMS $> 6$ nT (90 eV/cc) on the 10-min interval and maximum RMS higher than the average MSH RMS ($>150\%$). This threshold is applied for Fig. 8b. An event is regarded as continuous if the RMS exceeds the threshold with interrupts less than 10 min. We limit our study outward of the magnetosphere by a minimum of two values: (a) half the distance between the most distant Earth MP and the closest Earth bow shock (BS) at the same orbit, (b) $3 R_E$ outward from the most distant MP. We exclude single RMS spikes, which clearly correspond to the main magnetic field jumps at the MP. The reader can find early one-year Interball-1 TBL statistics in Savin et al. (1999). We display the maximum RMS amplitude in an event in Fig. 8a, starting from RMS $\sim$10 nT. The average value of the RMS maximum is slightly less than 20 nT ($\sim$900 eV/cc) and the absolute RMS maximum is over 40 nT. The above mentioned near-MP data gap in the tail is schematically marked by the violet dot-shading on the $(X, Y)$ plane. There are two features we would like to outline:
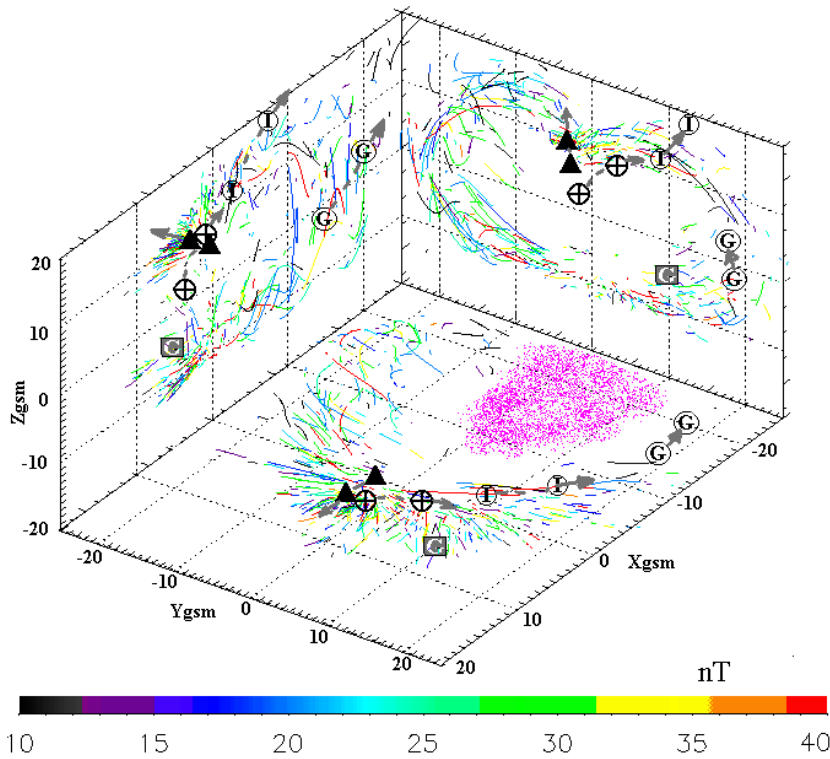
**Fig. 8a.** TBL in 1995–1998 from Interball-1 magnetic field data in 3 GSM planes. The full standard deviation is color-coded according to the scale at the figure bottom and shown at the pieces of orbit traces of Interball-1 (see the TBL definition in the text). The violet dot-shading marks lack of Interball-1 orbit coverage of the MP. Case studies are shown by symbols (circled crosses and triangles – for Polar and Interball-1 on 29 May 1996, for the remainder of the $t$ symbols, see the text).

– the near-cusp indentation visible in the northern TBL in the $XZ$ and $YZ$ planes; this indentation corresponds to the MP case reported in the OT by Savin et al. (1998b) and Urquhart et al. (1998). The TBL on 29 May 1996, displayed in Plates A2 and B1, is namely at the bottom of this indentation (the respective orbits are depicted by triangles for Interball-1 and crossed circles for Polar).

– the TBL "wings", ranging from the near-cusp TBL into the tail down to $X \sim -20 \, R_E$; these "wings" are in the vicinity of the boundary between the open mantle lines and the closed LLBL lines. The local minimum in the total magnetic field and currents providing field rotation from the open to closed lines are anticipated there.

The TBL events concentrate at high latitudes ($|Z| > 4 \, R_E$) near the OT and downstream of it; it is especially visible for variations with RMS $> 20 \, \text{nT}$. On the $YZ$-plane at low latitudes one can also recognize groups of intensive events (for both positive and negative $Y$); the $XZ$-plane demonstrates that most of them are encountered in the tail. Recently, Maynard et al. (2001) demonstrated the penetration of the MSH plasma into the tail "sash" in conjunction with the flank TBL. Note that although in Klimov et al. (1997) and Savin et al. (1997) the TBL-like signatures in the tail have been reported, nobody knew if this TBL is present there more or less permanently. Savin et al. (2002a) have demonstrated that a substantial part of the events in those "wings" at the higher latitudes is independent on the interplanetary (IMF) $B_y$, which contradicts the "sash" predictions. Approximately another half of the "wing" events follows the

"sash" $B_y$-dependence (cf. the above mentioned low-latitude events). The higher-latitude "wings" are in the vicinity of the boundary between semi-open mantle lines and closed LLBL lines; the local minimum in the total magnetic field and currents providing field rotation from the open to closed lines are anticipated there. In Fig. 8b we display now in 3 GSM planes the color-coded distribution of the events with magnetic RMS$>6 \, \text{nT}$ as a function of IMF $B_z$; the colors for respective $B_z$- intervals are depicted in the figure left lower corner. In the tail "wings" at negative $X$ the TBL is registered on longer orbit pieces for the northward IMF (red lines) compared with that of southward IMF (yellow lines), while the number of cases for both IMF $B_z$ is comparable. We would like to highlight that for IMF $B_z > 0$, namely at negative $X$, the anti-parallel magnetic fields are believed to reconnect. The presence of the shorter disturbed sites near the tail MP conforms to both the secondary fluctuating field reconnection at small scales and the TBL per se downstream of the throat obstacle. Thus, the presence of TBL "wings" for any IMF direction invokes the MSH plasma penetration not only in the cusp-shaped dayside region, but in the wider one (cf. Haerendel et al., 1978). This is valid in both cases: if turbulent diffusion provides the necessary mass transport and/or if the turbulence serves as the indicator of the local reconnections.

For the "magnetic bubbles" statistics Savin et al. (1999) uses the maximum depths of the spiky drops in total magnetic field ($|\boldsymbol{B}|$). We believe that the $|\boldsymbol{B}|$ drops are accounted for the diamagnetic effect of the heated MSH plasma inside
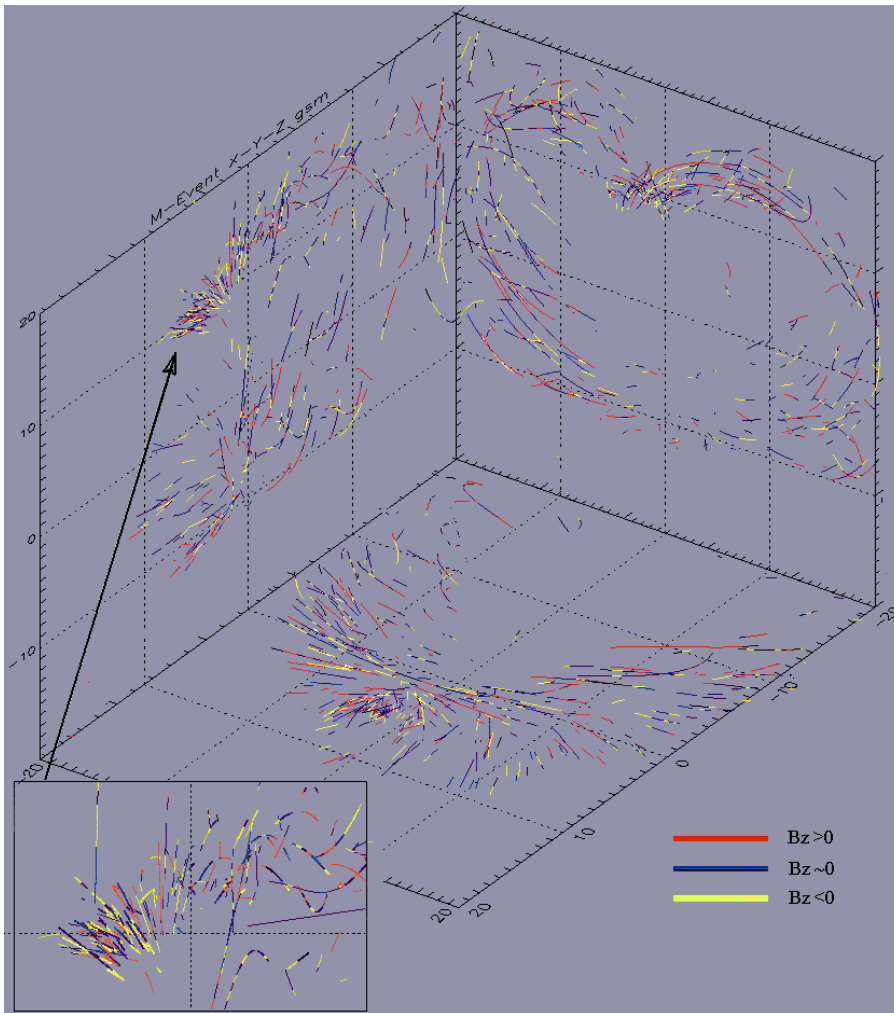
**Fig. 8b.** TBL in 1995–1998 from Interball-1 magnetic field data in 3 GSM planes for the full standard deviation >6 nT. The IMF $B_z$-dependence is color-coded according to the scale at the bottom of the figure and shown at the pieces of orbit traces of Interball-1 (see the TBL definition in the text); red color – $B_z > 2$ nT, yellow color – $B_z < -2$ nT, blue color – $B_z$ between 2 and −2 nT. The insert in the left bottom corner shows higher resolution of the near-cusp TBL from the plane ($XZ$) as shown by the arrow. Note the lack of Interball-1 orbit coverage of the MP, marked by violet dot-shading in Fig. 8a.

the "magnetic bubbles", that agrees with the Polar data in Plate B1(a, d). The "bubbles" distribution (not shown) is generally the same as the RMS in Fig. 8. The averaged maximum plasma pressure excess in "magnetic bubbles", for example, the March 1997 – March 1998 period, is d(NT)= 2160 eV/cc, the absolute maximum of the d(NT) reaches 7000 eV/cc. The magnetic field inside the "bubble" is 8.3 times weaker than outside. Taking plasma density in TBL of 5–10 1/cc, one obtains plasma heating of 220–430 eV inside the "magnetic bubbles", i.e. heating of 1.5–3 times relative to the temperature of the MSH ions. This is in good correspondence with predictions of Haerendel (1978). Intensive heating in the high latitude tail "wings" is seen only up to $X = -6 R_E$ (Romanov et al., 1999). As for the low latitudes, there are a number of intensive events, for example, from Geotail data on 27 January 1997 (circles "G", see next section) and on 27 August 1995 (squared white "G"); the latter occurred during highly disturbed conditions (see also Fig. 3a and related discussions).

We would like to finish this section by performing an inspection of the TBL occurrence near the northern cusp for different IMF $B_z$ in Fig. 8b. The reason is that, for example,

Russell et al. (1998) proposed that the case under study at dominant IMF $B_z > 0$ differs from those with different IMF, while Fig. 8a demonstrates that the TBL encounters by Polar on this day are just at the bottom of the average indentation over the cusp (it would shift into the middle of the TBL locus if one corrects the Polar position by the ratio of 1/6 power of the extremely high SW dynamic pressure on 29 May 1996 to that of the average SW dynamic pressure). The insert in the lower left corner in Fig. 8b shows higher resolution of the TBL cases over the northern cusp. For positive $X$ (left part of the Insert) the number of events with IMF $B_z > 0$ (red lines) constitute ∼75% of those with negative $B_z$, with no tendency for the former ones to be seen farther away from the Earth. Near the tail MP (right side, upper quadrant) the number of events shows little or no dependence on $B_z$, while for the northern IMF the TBL events have a longer duration. The outlined peculiarities infer only a weak dominance of the TBL encounters at the places with on average anti-parallel magnetic fields (at the sunward OT border for $B_z < 0$ and tailward of the cusp for $B_z > 0$, see Plate A3). The $(Y, Z)$ plane in Fig. 8b demonstrates a clear indentation over the northern cusp for any IMF $B_z$. Thus, we suggest that the

sunward flows over the cusp during IMF $B_z > 0$ can affect the MP shape, etc., as proposed by Russell et al. (1998), but in rather narrow ranges of $Y$ (see respective discussion in previous section), that practically is not visible in the average TBL maps in Fig. 8. So, we regard the MSH/cusp transitions on 29 May 1996 as representative ones in the most general aspects.

## 6   Discussion and conclusions

In this paper we have presented primarily only one case of multi-spacecraft data comparison, i.e. 29 May 1996, but this case demonstrates the general features of the TBL. The uniqueness of the stable and dominant IMF $B_z > 0$ allows us to compare quantitatively the high-shear TBL on Interball-1 ($\sim$03:16 UT) and on Polar ($\sim$07:00 UT, cf. Savin et al., 1998b) with the low-shear TBL on Polar (at $\sim$04:00 UT, cf. Romanov et al., 1999), using Interball-1 as the upstream MSH monitor. Here we discuss the achievements of Interball-1 and other contemporary missions in exploration of the MSH-cusp interface on the basis of both the data presented above and of the already published results.

### 6.1   Common properties of turbulent boundary layer

An inspection of the TBL crossings by Interball-1 (Fig. 8a) shows that on 29 May 1996 the TBL, as determined by Polar and Interball, is closer to the Earth than it is on other days, but this can be explained by an unusually high MSH density (see Fig. 6 and Urquhart et al., 1997). In the $(XY)$ plane the TBL trace is observed just near noon, as shown in Fig. 8. Both the case study and its comparison with the MHD model and with the map of the TBL in 1995–1998 show that the interaction of MSH flows with the high latitude MP is neither smooth nor laminar. The interaction produces a layer with strong nonlinear turbulence – the TBL. It is not limited by the near-MP part of the stagnation region over the cusps (see Plate A1), but spreads tailward until $X$ about $-20\,R_E$, maximizing along the transition region from the mantle to the low latitude boundary layer. Three-year Interball-1 data show that the TBL is present in $\sim$80% of the cases (with average amplitude $\sim$20 nT). Most TBL-like events are seen at high latitudes, i.e. at $4 < |Z| < 15\,R_E$. The most intense events could be approximated by the effective disk with diameter of $6\,R_E$ above the dayside cusps, with an average maximum RMS of about 22 nT (see Savin et al., 1999). The minor part of TBL-like crossings goes down to the equator; the "sash" is proposed as a TBL source on the tail flanks (Maynard et al., 2001). Examples of Geotail data also show that the turbulence level, both at the dayside and low-latitude tail field lines, might be high enough in comparison with the average TBL turbulence level over the cusps, especially under disturbed SW conditions. Essential MSH plasma heating ($\sim$300 eV) occurs in $\sim$80% of the cases within the TBL "magnetic bubbles" (cf. $T_i$ rising in Plate B1 in the zone with the "bubbles"). The magnetic field in the "bubbles" is

highly reduced (8.3 times on average). Some of the magnetic bubbles are transported across the MP (Savin et al., 1998b, 1999, 2002a; Romanov et al., 1999), constituting a mechanism for inward plasma transport. The RMS magnetic field intensity has a tendency to fall tailward in the TBL "wings" that expand into the tail (Fig. 8). Intense heating is seen until $X = -6\,R_E$ (Romanov et al., 1999). The TBL "wings" indicate the possibility of MSH plasma penetration into a wider region than just over the dayside cusps (cf. Haerendel et al., 1978; Savin et al., 1999). A substantial number of TBL encounters do not depend on IMF $B_y$ and $B_z$ (see Fig. 8b and Savin et al., 2002a) that highlights the importance of the effects, which are not relayed with the reconnection of on average anti-parallel magnetic fields.

### 6.2   Multi-scale reconnection

On 29 May 1996, the data display typical TBL features (Plates A2 and B1): wideband intensive magnetic nonlinear fluctuations (with energy density up to 33% of full plasma energy density in flowing MSH), "diamagnetic bubbles" with $|\boldsymbol{B}|$ drops from $\sim$100 nT down to a few nT (Fig. 6), plasma heating and nearly Alfvénic field-aligned jets, etc. (cf. Savin et al., 1998b, 1999, 2002b; Sandahl et al., 2000; Stasiewicz et al., 2001; Dubinin et al., 2002). We suggest that the high absolute disturbances during this day can result from the high MSH energy density ($\sim$15 keV/cc on Polar versus 2–3 keV/cc for average Interball-1 crossings). Both maximum and average $T_i$ growths in the Polar inbound TBL (at $\sim$07:00 UT) are $\sim$2 times higher than those in the low-shear TBL (at $\sim$04:30 UT). The ion heating ($\sim$3 times) at $\sim$04:30 UT in Plate B1 corresponds to the Interball-1 average ion heating (Savin et al., 1999). We attribute this visible difference in the ion heating and doubling of the fluctuation power to the local annihilation of the anti-parallel average fields inside/outside the MP. Later in this section we refer to this as "primary cusp reconnection". Its characteristic scale is estimated as 1000–2000 km (see Fig. 3a and 4a and related discussions above). Savin et al. (1998b) suggested that such merging might contribute to the TBL energetics along with the smaller scale bursty reconnection of fluctuating fields (of $\sim$ hundreds km). The sunward Alfvénic jets represent direct evidence for the merging (Fig. 6). Input from local processes is confirmed by the out-flowing Poynting flux (Plate B2). On the other hand, the wide and long current sheet in Plate A4 upstream of the remote reconnection site (RRS) infers possible continuation of the TBL from the cusp throat to the RRS (Plates A1, A3).

A possible geometry of anti-parallel merging in the TBL is depicted in Plate A3. We approximate the MP grid by a smooth function adjusted to the MP crossing positions and respective MP normals (see Savin et al., 1998a), with the distance to the subsolar point corresponding to the average SW dynamic pressure from 03:00 to 07:00 UT. A comparison of the measured normals with the model of Urquhart et al. (1997) shows that the model does not reproduce the normal inclination towards the noon meridian, which is

especially substantial in the case of the Polar outbound crossing at 04:09 UT. To determine the qualitative effect of the measured normals on the magnetopause shape we have chosen the disturbance to the average symmetric (relative to $X$) MP surface ($R0$, see Urquhart et al., 1997) with the subsolar point at $X = 7.5 R_E$ in the form:

$$R0/R = 1 + 0.24 \exp\left(-\left(((L - 60)/7)((F - 90)/15)\right)^2\right) +$$
$$0.25 \exp\left(-\left(((L - 77)/15)((F - 88)/60)\right)^2\right),$$

where $L = \arccos(X/R0)$, $F = \operatorname{arctg}(Z_{GSM}/Y_{GSM})$ in degrees. The parameters for the disturbance have been chosen from the best fit to the three MP crossings (see Sect. 2) and to reproduction of the normal behaviours. The MP normals are shown by thick blue arrows at the positions of the main MP current sheets (Savin et al., 1998a). At the bottom of Plate A3 we show the full length of the normal vector of 6 $R_E$ (i.e. the shorter normal has a projection perpendicular to the plate plane). Interball and Polar orbit traces are depicted in Plate A3 by the dashed violet and brown arrows, respectively. The approximate position of the model "remote reconnection site" is marked by the framed "RRS" in Plates A3 and A4. The original magnetospheric field lines are marked by green, and those of the IMF by red. The framed "Mantle" stands for the mantle-like ions flowing tailward along field lines at ~02:30–03:00 UT in Plate A2(a). A blue grid outlines the average MP indentation. The most intense TBL from Fig. 8 is schematically displayed by green dot shadowing. The disturbed wavy reconnected lines are shown near the center of the smooth MP indentation. This reflects the measured, nearly anti-parallel magnetic fields across the MP at ~07:00 UT in Plate B1 and Fig. 6 with the wave-train TBL transition (see also Plates B3–5). Our comparison of the measured and model data, along with the high-resolution ion data analysis on Interball by Avanov et al. (2001), support that the model merging (RRS) is located at approximately the predicted location. Certainly, a crude model grid is unable to reproduce the wavy jet fine structure.

The anti-parallel field situations for very different IMF can be found almost always in the outer cusp throat because of magnetic field elongation over the indented MP by the high-beta MSH flow. At the same time, anti-parallel fields are usually seen away from the outer cusp throat at the smooth MP (i.e. in the RRS) as well. For northern IMF a case with (at least) two anti-parallel merging sites is illustrated in Plate A3. Savin et al. (2002a) presented a similar picture for the southern IMF; the Magion-4 statistics of the sunward flows in the exterior cusp for IMF $B_z < 0$ provide a strong indication of the local cusp reconnection.

Fedorov et al. (2000), Dubinin et al. (2002), Safrankova et al. (1998) and Merka et al. (2000) also provided experimental evidence for local penetration of the MSH plasma at high latitudes in the cusp vicinity. Belmont and Rezeau (2001) developed the linear theory, which predicts that strong ULF fluctuations that occur just outside of or at the magnetopause, can independently result in micro-reconnection and

local plasma penetration all along the magnetopause surface even in the absence of quasi-stationary macro-reconnection of anti-parallel magnetic fields. In our presentation we outlined highly deflected (especially in the $Y$ direction, see Plate B1(b) and comparison with the model above), almost Alfvénic flows in the outbound TBL at about 04:30 UT for quasi-parallel magnetic fields at the MP. Because annihilation of the average field is not possible there, we attribute these features to the by-product reconnection of the fluctuating fields in the TBL. A possibility is that secondary reconnection of the fluctuating fields in the TBL (regardless of the origin of the TBL) can provide the plasma inflow in the quasi-parallel case. This reasoning is along the lines of the Haerendel (1978) predictions and findings of Savin et al. (1998b) for other IMF directions. The reconnection bursts can provide a particular mechanism for the effective "interconnection of the parallel fields" (see Chandler et al., 1999 and references therein). On the other hand, the micro-reconnection creates the specific structure of the MP current sheet(s) with magnetic islands, which results in plasma percolation through the nonlinear boundary network (Kuznetsova and Zelenyi, 1990). The order-of-magnitude estimate shows that this stochastic plasma transfer through the TBL/cusp walls might provide a means of populating both the cusp and low latitude boundary layer (LLBL): the diffusion coefficient $D_P \sim (5 - 10)10^9$ m$^2$/s for typical MP parameters results in a particle influx of $(1 - 2)10^{27}$ particles/s (Savin et al., 1999). Primary cusp reconnection should certainly amplify the plasma inflow. Summarizing the discussion above, on 29 May 1996 multiple reconnection sites might operate simultaneously:

– Remote (from the cusp) reconnection site (RRS) that is predicted by the MHD model (Fedder et al., 1995) and the scale of which can be evaluated up to a few Earth radii;

– Primary cusp reconnection site(s) at the location of the anti-parallel average fields (of $\sim$ few thousand km), where local magnetic field annihilation enforces the fluctuation level and heating;

– Secondary reconnections of the highly fluctuating fields potentially at all locations within the TBL, that can occur at small scales (down to an ion gyroradius) even for the low-shear average fields (cf. Haerendel 1978; Savin et al., 1998b; Chandler et al., 1999).

In Plate A3 these three types of reconnection are shown schematically by laminar reconnected lines marked "RRS", wavy reconnected lines in the TBL and green dot shadowing, respectively.

## 6.3 Local versus remote mechanisms of magnetosheath plasma penetration into cusps

Despite the problem of MSH plasma penetration being far from its final solution, we would like to discuss the experimental evidence for the operation of local cusp processes.

The cusp at different altitudes and latitudes as observed by Polar, Interball-1, HEO 95-034, and DMSP F12 and F13 seems to be rather far from field lines of the RRS traces (Fig. 7). As we have mentioned above, the cusp can hardly be populated by the MSH plasma, which enters the MP on the tail field lines only. Local penetration by the MSH plasma on the dayside field lines should be involved, for example, at 04:00 UT in Plate B1 and in the dusk cusp on HEO in Fig. 7 (see related discussion above, cf. "entry layer" by Paschmann et al., 1976). Savin et al. (1998a) have pointed out that the observation of the TBL at three points in the range 08:30–15:00 MLT and 57–670 of geomagnetic latitude over a period of 4 h is a strong argument for a temporally-persistent existence of this TBL (see also Fig. 7). As the RRS trace moves in the range 16:00–01:00 MLT and 80–900, the stable TBL seems to be a more appropriate widespread source for the cusp on 29 May 1996. The MHD model depicts the access of the upstream MSH flows deep inside the outer cusp throat (dominated by $V_x < 0$ in Plate B1(b), see discussion above). Similar to the cases with IMF $B_z < 0$ from Savin et al. (1998b), these flows interact with the tailward outer cusp throat. On the other hand, the sunward flows with reconnected kinked field lines are predicted and actually observed but only in very narrow regions over the OT. Thus, we assume that, although this remote reconnection process operates, its relative importance might be small in comparison with the permanently operating TBL primary and secondary mergings.

Onsager et al. (2001) provided arguments from the electron HYDRA data that at 04:08–04:20 UT Polar has generally been on the double-reconnected field lines outside the MP (see their Fig. 6), which should be a consequence of the large-scale RRS. However, at this time the ions, moving along the magnetic field lines, are the same as in the MSH (excluding the short period of negative magnetospheric-like $B_z$), while the antiparallel ions are mostly heated (presumably in the MP current layer). The latter infers connection to the northern cusp through the MP (TBL). For the double-reconnected lines the same antiparallel heated ions should be seen at least after the time-of-flight period. For characteristic ion energy ~1 keV the time-of-flight is ~6 min, i.e. two times shorter than the time interval 04:08–04:20 UT. In this situation we would like to account for electron heating in the parallel and antiparallel directions in the TBL by positioning Polar inside the distributed region of electron acceleration. In fact, the bi-directional electron flows can be seen in different configurations:

– on the closed (at least for electrons) field lines, i.e. namely what Onsager et al. (2001) assumed;

– on the line that connects the ionosphere at one end and touches the electron acceleration region at the other end. For such a configuration the accelerated electrons should be reflected from the convergent part of the field line near the ionosphere in a few seconds and for a stable heating source constitute the bi-directional parallel-heated distribution (cf. Savin et al., 1998b);

– when the electron heating source is distributed or multiple, i.e. seen from both parallel and antiparallel field directions.

To distinguish the spacecraft located at the closed field lines or inside the regions of electron acceleration we compare the electron distributions from Onsager et al. (2001) with wave data shown in Fig. 2. Savin et al. (1997, 1998b) demonstrated that intense waves near the lower hybrid frequency (i.e. ~ several Hz in the TBL) can accelerate electrons along field lines up to the measured energies. Figure 2 clearly demonstrates that at 04:08–04:20 UT strong wideband waves are seen up to the electron cyclotron frequency. Panels (a) and (c) especially display waves at 5–20 Hz. Thus, the wave data support that electrons in the TBL can be accelerated by the intense ULF waves. It seems that outside the TBL the field topology tracing by electrons could be applied successfully, while distinguishing between options 1 and 2 still remains to be done.

In the TBL on Polar $T_i = 400 - 600$ eV at 03:20–04:25 UT (see Fig. 7a and Plate B1e), which are close to pre-noon ion energies measured on HEO, at 01:35–03:15 UT (see Fig. 4 in Grande et al., 1997) and to those in the cusp on Interball at 01:35 UT (Plate A2a). The Polar TBL at 06:50 UT with $T_i$ up to 900 eV seems to be an appropriate source for the afternoon mid-altitude cusp on HEO with the average ion energy also ~900 eV. These data provide further evidence that in the mid-altitude cusp the MSH plasma supply can be controlled by the local acceleration/heating processes in the respective TBL over the cusp.

We would like to outline further possible consequences of the permanent TBL presence over the cusps. The intense plasma mixing in the TBL can effectively supply ions to the inter-connected flux tube portions, which are close to the MP from the MSH side (cf. "eddy convection" of Haerendel, 1978, see also Fig. 6 and related discussions). This should enforce effective MSH plasma inflow through the inter-connected field lines after the termination of merging (cf. Fedorov et al., 2000). The MP current sheet presumably reflects the electrons and lower energy ions, which have their gyroradii smaller than the sheet/kink characteristic scale (cf. Savin et al., 1998b).

## 6.4 Interaction of magnetosheath flows with the outer cusp throat

Now we would like to address another primary mechanism for the energy and mass transfer at the MSH/cusp interface: the direct interaction of the MSH flow with the outer cusp throat (OT). From Fig. 8 and Plates A1, A3, and A4 we see that the MP indentation might present a substantial obstacle for the plasma flow streaming around the MP.

The supersonic flow burst just outside the MP (see Plate A2) can be suggestive of a cusp "Laval nozzle" (Fig. 1), according to the theory of Yamauchi and Lundin (1997). However, we believe that the "rising flank of the tail lobe" presents an obstacle to the MSH flow in the vicinity of the

magnetopause (Paschmann et al., 1976), or, in other words, it represents an "almost vertical outer cusp throat tailward wall" (Savin et al., 1998b). The obstacle slows down and diverts the magnetosheath flow, so that the turbulent boundary layer originates in the stagnation region in front of the obstacle and in its wake (Haerendel, 1978). Yamauchi and Lundin (1997) proposed that the ionospheric ion outflow is the reason for the MSH flow velocity jumping back to a subsonic value. While Polar registered oxygen and He$^+$ outflow in the outer cusp and TBL (Grande et al., 1997), we suppose that this plasma loading is not the primary cause: the ionospheric particles have negligible contribution to the average mass and energy densities, while both the DC magnetic field pressure ($Em$) at the OT wall and in the TBL spikes reach the magnitude of the ion energy density, $Es (\sim E_{\text{thermal}}$ in the Polar case), in the MSH (see Plates A2(d), B1(d) and Savin al., 1998a, b). Both the outer cusp throat and TBL are permanent features of the high latitude magnetopause. Savin et al. (1998a) suggested that the rotational discontinuity (Plate A2(b, d) and Fig. 1) separates the reconnected and entirely magnetosheath field lines, which agrees with $B^2/8\pi$ dominating in this region. In the latter case the RD could represent the outer wall for the "Laval nozzle" that seems to add an element, which has not been specified yet, to the model of Yamauchi and Lundin. Figure 3 in Savin et al. (1998a) displays an IMF discontinuity $\sim$ at the time of the RD. However, as IMF $B_y$ changes in the opposite sense to that observed on Interball, we suppose that the SW parameters changed through the discontinuity, and in turn caused the RD displacement earthward.

Multi-point data on 27 January 1997 (Savin et al., 1998c) provide an opportunity to obtain the quantitative estimate for the drop in the kinetic energy density, $E_{kin}$ (relative to the thermal one, $E_{\text{thermal}}$) due to the MSH flow interactions with the tailward cusp wall. The model of Spreiter and Stahara (1980) predicts the gain of $E_{kin}/E_{\text{thermal}}$ to be $\sim$2 for Geotail relative to Interball-1 in Fig. 4 of Savin et al. (1998c) at $\sim$11:20 UT, while the measured gain is $\sim$8, i.e. $E_{kin}/E_{\text{thermal}}$ drops by a factor of $\sim$4 at high latitudes in comparison to the simultaneously obtained low latitude values, re-calculated for the same $X$. Following Haerendel (1978) we address this deceleration to the MSH flow interaction with rising field lines at the tailward wall of the outer cusp throat. The sound Mach number in the unperturbed MSH ($M_s \sim 2.1$) drops to $M_s < 1$ downstream of the cusp obstacle on 21 April 1996 (Savin et al., 1998b). $M_s \sim 2$ is also seen in the Interball-1 data just outside the MP (Plate A2), while the flow/discontinuity geometry in the cusp throat is not clear enough yet. The $M_s$ supersonic/subsonic transitions are compatible with the existence of slow/intermediate shocks (see, e.g. Russell 1995 and references therein) in the vicinity of the tailward cusp wall (cf. Yamauchi and Lundin, 1997; Savin et al., 1998b). Thus, we think that the finding of the MSH flow deceleration/heating downstream of the high latitude cusp represents a valuable result from the multi-spacecraft ISTP data that outlines the significance of the bulk flow energy transformation in the process of the flow inter-action with the outer cusp throat.

For the comparison of transient events at high and altitudes, ion back-tracing should be modified to include scattering and reflection of ion flows in the TBL. We would like to point out also that the TBL not only regulates the penetration of the "remote" (e.g. from RRS) ion flows, but also provides both plasma penetration from the MSH and secondary magnetic flux reconnection. This magnetic flux, reconnected at small scales, on average, is capable of driving magnetospheric convection (Haerendel, 1978). In fact at this point we touch an open critical problem of the SW/magnetosphere interaction: where are the Earth magnetic field lines being opened? Our current understanding is that this process is one of multi-point and multi-scale. We believe that the MSH/cusp interface plays the dominant role at least in quasi-steady conditions.

The tilt angle dependence of the cusp position both at high and low altitudes (Zhou et al., 1999; Merka et al., 1998; Smith and Lockwood, 1996) has a natural explanation if the TBL is a general source of plasma for the cusps:

(a) the higher the tilt (i.e. the closer the dipole axis to the Sun), the more open the OT for the external MSH flow (i.e. the OT tailward wall represents the steeper obstacle for the MSH flow);

(b) the higher the shift/penetrations at the OT tailward wall, the deeper the MSH plasma will be seen on the tail field lines;

(c) the deeper the plasma penetration (and/or tailward field line deflection), the more tailward it will be projected into the polar cap (i.e. the cusp is at higher invariant latitudes). Note that the tilt-related cusp shift has no explanation in the "traditional" global-reconnection approach.

6.5   Turbulent boundary layer sources and character

Following Haerendel (1978), we suppose that first of all the TBL results from the turbulent mixing driven by the regular MSH flow interaction with the deformed near-cusp magnetopause. The disturbed flows, accelerated in the remote reconnection site, can contribute to the TBL generation as well. The remote reconnection site also regulates the TBL position by shifting the MP indentation according to the SW parameters. Away from the plasma stagnation region in the OT center, the Kelvin-Helmholtz plasma vortices with secondary reconnections should provide a mechanism for plasma heating/transport (cf. Chen et al., 1997). The fluctuation level in the MSH, especially downstream of quasi-parallel bow shocks, is believed to stimulate the ULF turbulence generation in the TBL. In some cases mentioned above, the correlation at the time interval of $\sim$5–15 min in the post-BS region and the middle MSH, as well as in the OT reaches 0.6–0.7, and is a manifestation of the TBL/MP reactions to the SW/MSH transients. Thus, the transient current sheets and density gradients generated by dynamic

SW and/or MSH interactions with the MP should contribute in the TBL energy balance. We think that, as a whole, the TBL collects, transforms and generates the plasma flow and magnetic field disturbances simultaneously from several sources. Its status depends on the short-term time history of the SW/magnetosphere interactions, influencing, in turn, the interaction of the magnetosphere with newly-arriving disturbances at each particular moment.

Besides the transient/dynamic reactions of the TBL to external disturbances, the TBL appears to have well-defined inherent properties, which we have been fortunate to trace at different points of the MSH and MP boundary layers during the favorable period of relatively steady SW parameters. The modern wavelet technique provides us with strong evidence that the spectral characteristics of the TBL on 29 May 1996 are very well defined. The simultaneous Interball/Polar magnetic field data demonstrate the presence of a maximum at 1–2 mHz throughout the MSH, TBL and inside MP (Fig. 3b). The amplification and frequency shift to higher values in the OT might be a local TBL feature (cf. Fig. 6 in Savin et al., 2002a). Taking the Alfvén speed in the MSH as a proxy for the phase velocity we obtain 6–8 $R_E$ as the characteristic scale, i.e. ∼ the size of the dayside MSH or cusp field lines that could imply detecting of long period surface waves (cf. Savin et al., 1998b; Sandahl et al., 2000). Such long waves can pass through the MP (see Plate B3) and might resonate with the dayside flux tubes in the PC 4–5 range or at higher harmonics (cf. Pilipenko et al., 1999). The most pronounced TBL waves at 0.005–0.5 Hz have the characteristic kinked shapes and slopes (Fig. 3b). The spectral power here is much higher than that of fluctuations in the flowing and stagnant MSH and the spectral shape is also different. We have checked the waves in the TBL on 26 August 1995, 19 and 23 June 1998 and found that the kinked shape with slopes of 1–1.5 and 2–2.6 are characteristic for the TBL. Spectral peaks at lower frequencies might also appear. A substantial TBL feature, which we think occasionally coincides with a simultaneous one in the MSH in Fig. 3b, is the frequency of the kink (cf. asterisks and crosses). Thus, the characteristic time/space scale, which corresponds to the kink, might be thought to originate uniquely in the MSH. However, the Polar data just over the TBL at 05:00–05:45 UT show practically no kink and, thus, do not confirm this suggestion. We would like to attribute the kinked MSH spectra on Interball at 04:08–04:39 UT, for example, to effects of MSH disturbances, such as intermediate/slow shocks detached from the MP (cf. Russell, 1995), rather than regard them as a common MSH property.

The higher value of the slope in the TBL of ∼2 is close to that characteristic for the developed self-consistent kinetic turbulence in the geomagnetic tail; similar to the near-Earth neutral sheet during substorms, the lower slope of about 1 might be attributed to the flickering noise (see Zelenyi and Milovanov, 1998 and references therein).

Cascade-like wavelet and bicoherence spectrograms and wavelet correlation time infer coherent, most probably, three-wave, interaction between wave trains, while the disturbances seem to be random in the waveforms (Figs. 5–6 and Plates B3–B6). The local wave trains originate from the interaction of the disturbed MSH flows with the MP. Their dispersion is indicative for kinetic Alfvén waves (KAW, see Fig. 3a). Johnson and Cheng (1997) proposed excitation of transverse KAW at the MP by interaction of the compressible MSH waves with the current sheet. Later, Belmont and Rezeau (2001) demonstrated the growth of the trapped large-amplitude KAW inside the non-uniform current sheets. At the nonlinear stage the Alfvénic disturbances in the TBL modulate the incident MSH flow in a self-consistent manner, being globally synchronized by phase coupling with the large-scale variations (at ∼3 mHz, see Plate B3–B6). While linear KAW resonances (i.e. singularities in the equations of Belmont and Rezeau, 2001) are absent, we suggest that the coherent large-scale structures can originate from the inverse KAW cascades (cf. Plates B3, B5, B6 and Fig. 5b). Thus, the chain is closed: the TBL seems to be a multi-scale self-organized system of interacting nonlinear waves. This infers a qualitative difference from the traditional approach wherein the MSH/cusp interaction is regarded as a linear superposition of magnetospheric responses on the solar wind or MSH disturbances. Note also that the long-term correlation is suggestive of systems out of equilibrium near the critical point (cf. Consolini and Lui, 2000). The kinked TBL spectra with characteristic slopes remarkably resemble those in the near-Earth neutral sheet in the state of the self-organized criticality (see e.g. Zelenyi and Milovanov, 1998).

## 6.6 Concluding remarks

The results of our data analysis strongly indicate that the TBL fluctuations, instead of being random, are highly correlated and organized by the cascades of nonlinear interactions. The selected coherent wave trains are capable of synchronizing interactions throughout the TBL, somewhat resembling a global TBL resonance (cf. "Alfvén resonator" assumed by Stasiewicz et al., 2001). Multiplying the characteristic period of the "organizing" wave mode (at ∼3 mHz) by the MSH Alfvén speed we obtain 3–4 $R_E$ as a proxy for the characteristic scale. This is close to the diameter of the TBL or outer cusp throat (Plates A1, A3) and can be attributed to a standing nonlinear wave, trapped in the outer cusp throat.

We suggest that multi-scale TBL processes play at least a comparable role to those of reconnection remote from the cusp in the solar wind energy transformation and population of the magnetosphere by the MSH plasma.

# References

Anderson, R. R., Harvey, C. C., Hoppe, M. M., Tsurutani, B. T., Eastman, B. T., and Etcheto, J.: Plasma waves near the magnetopause, J. Geophys. Res., 87, 2087, 1982.

Angelopoulos, V., Mozer, F. S., Bonnell, J., Temerin, M., Somoza, M., Peterson, W. K., Collin, H. L., and Giles, B.: Wave power studies of cusp crossings with the Polar satellite, J. Geophys. Res., 106 (A4), 5987, 2001.

Avanov, L. A., Smirnov, V. N., Waite, Jr., J. H., Fuselier, S. A., and Vaisberg, O. L.: High-latitude magnetic reconnection in sub-Alfvénic flow: Interball Tail observations on 29 May 1996, J. Geophys. Res., 106, 29 491–29 502, 2001.

Belmont, G. and Rezeau, L.: Magnetopause reconnection induced by Hall-MHD fluctuations, J. Geophys. Res., 106 (A6), 10 751–10 760, 2001.

Belova, E. V., Blecki, J., Denis, M., Zelenyi, L. M., and Savin, S. P.: Excitation of ion cyclotron waves at the boundary of the magnetosphere, Sov. J. Plasma Phys., 17, 555, 1991.

Blecki, J., Rothkaehl, H., Kossacki, K., et al.: ULF-ELF-VLF-HF Plasma Wave Observations in the Polar Cusp Onboard High and Low Altitude Satellites, Phys. Scripta, 75, 259–263, 1998.

Chandler, M. O., Fuselier, S. A., Lockwood, M., and Moore, T. E.: Evidence of component merging equatorward of the cusp, J. Geophys. Res., 104, 22 623, 1999.

Chen, S.-H., Boardsen, S. A., Fung, S. F., Green, J. L., Kessel, R. L., Tan, L. C., Eastman, T. E., and Craven, J. D.: Exterior and interior polar cusps: Observations from Hawkeye, J. Geophys. Res., 102 (A6), 11 335, 1997.

Chen, Q., Otto, A., and Lee, L. C.: Tearing instability, Kelvin-Helmholtz Instability and Magnetic Reconnection, J. Geophys. Res., 102 (A1), 151, 1997.

Consolini, G. and Lui, A. T.: Symmetry breaking and nonlinear wave-wave interaction in current disruption: possible evidence for a phase transition, in: Magnetospheric Current Systems, Geophysical Monograph 118, American Geophysical Union, Washington D.C., pp. 395–401, 2000.

Dubinin, E., Skalsky, A., Song, P., Savin, S., Kozyra, J., Moore, T. E., Russell, C. T., Chandler, M. O., Fedorov, A., Avanov, L., Sauvaud, J. A., and Friedel, R. H. W.: Polar-Interball coordinated observations of plasma characteristics in the region of the northern and southern distant cusps, J. Geophys Res., 107, A5, 10.1029/2001JA900068, 2002.

Fedder, J. A., Lyon, J. G., Mobarry, C. M., and Slinker, S. P.: Topological structure of the magnetotail as a function of interplanetary magnetic field direction, J. Geophys. Res., 100, 3613, 1995.

Fedorov, A., Dubinin, E., Song, P., Budnick, E., Larson, P., and Sauvaud, J. A.: Characteristics of the exterior cusp for steady southward IMF: Interball observations, J. Geophys. Res., 105, 15 945–15 957, 2000.

Fung, S. F., Eastman, T. E., Boardsen, S. A., and Chen, S.-H.: High-altitude cusp positions sampled by the Hawkeye satellite, Phys. Chem. Earth, 22, 653–662, 1997.

Grande, M., Fennell, J., Livi, S., et al.: Observations of the mid-Altitude Magnetosheath During a Persistent Northward IMF Condition: Polar CAMMICE Observations, Geophys. Res. Lett., 24, 1475–1478, 1997.

Haerendel, G. and Paschmann, G.: Entry of solar wind plasma into the magnetosphere, in: Physics of the Hot Plasma in the Magnetosphere, edited by Hultqvist, B. and Stenflo, L., 23, Plenum, NY, 1975.

Haerendel, G.: Microscopic plasma processes related to reconnection, J. Atmos. Terr. Phys., 40, 343–353, 1978.

Haerendel, G., Paschmann, G., Sckopke, N., Rosenbauer, H., and Hedgecock, P. G.: The frontside boundary layer of the magnetopause and the problem of reconnection, J. Geophys. Res., 83, 3195, 1978.

Johnson, J. R. and Cheng, C. Z.: Kinetic Alfvén waves and plasma transport at the magnetopause, Geophys. Res. Lett., 24, 1423, 1997.

Klimov, S. I., Nozdrachev, M. N., Triska, P., Vojta, Ya., Galeev, A. A., et al.: Investigation of plasma waves by combined wave diagnostic device BUDWAR PROGNOZ-10-INTERCOSMOS, Cosmic Research (Transl. from Russian), 24, 177, 1986.

Klimov, S., Romanov, S., Amata, E., Blecki, J., Büchner, J., et al.: ASPI Experiment: Measurements of Fields and Waves Onboard the INTERBALL-1 Spacecraft, Ann. Geophysicae, 15, 514–527, 1997.

Kuznetsova, M. M. and Zelenyi, L. M.: The theory of FTE: Stochastic percolation model, in: Physics of Magnetic Flux Ropes, edited by Russell, C. T., Priest, E. R., Lee, L. C., 473-488, American Geophysical Union, 1990.

La Belle-Hamer, A. L., Otto, A., and Lee, L. C.: Magnetic reconnection in the presence of sheared flow and density asymmetry: application to the Earth's magnetopause, J. Geophys. Res., 100, 11 875–11 889, 1995.

Lundin, R., Woch, J., and Yamauchi, M.: The present understanding of the cusp, in: Proceedings of the Cusp Workshop, European Space Agency, Spec. Publ., ESA SP-330, pp. 8-3-95, 1991.

Maynard, N. C., Savin, S., Erickson, G. A., Kawano, H., Nemecek, Z., et al.: Observation of the magnetospheric "sash" and it implications relative to solar-wind/magnetospheric coupling: A multisatellite event analysis, J. Geophys. Res., 106, 6097, 2001.

Merka, J., Safrankova, J., Nemecek, Z., Fedorov, A., Borodkova, N., Savin, S., and Skalsky, A.: High altitude cusp: INTERBALL Observations, Adv. Space Res., 25, 7/8, 1425–1434, 2000.

Ogilvie, K. W., Chornay, J. D. , Fritzenreiter, R. J., Hunsaker, F., Keller, J., et al.: A comprehensive plasma instrument for the WIND spacecraft, in: The Global Geospace Mission, Space Science Rev., 71, pp. 55–77, 1995.

Onsager, T. G., Scudder, J., Lockwood, M., and Russell, C. T.: Reconnection at the high latitude magnetopause during northward IMF conditions, J. Geophys. Res., 106, 25 467–25 488, 2001.

Paschmann, G., Haerendel, G., Sckopke, N., Rosenbauer, H., and Hedgecock, P. C.: Plasma and magnetic field characteristics of

the distant polar cusp near local noon: The entry layer, J. Geo-
phys. Res., 81, 2883, 1976.

Petrinec, S. M. and Russell, C. T.: An examination of the effect
of dipole tilt angle and cusp regions on the shape of the dayside
magnetopause, J. Geophys. Res., 100, 9559–9566, 1995.

Pickett, J. S., Gurnett, D. A., Menietti, J. D., LeDocq, M. J., Scud-
der, J. D., et al.: Plasma Waves Observed During Cusp Energetic
Particle Events and Their Correlation with Polar and Akebono
Satellite and Ground Data, Adv. Space Res., 24, 23, 1999.

Pilipenko, V., Fedorov, E., Mazur, N., Engebretson, M. J., and
Hughes, W. J.: Magnetohydrodynamic waveguide/resonator for
Pc3 ULF pulsations at cusp latitudes, Earth Planets Space, 51,
441–448, 1999.

Pottelette, R. M., Malingre, N., Dubouloz, B., Aparicio, et al.: High
frequency waves in the cusp/cleft regions, J. Geophys. Res., 95,
5957, 1990.

Romanov, S. A., Klimov, S. I., and Mironenko, P. A.: Experimental
Derivation of ELF. Wave Dispersion Relations and Evidence of
Wave Coupling in the Earth Bow Shock Foot from the Data of
the PROGNOZ-10, Adv. Space Res. 11, 19, 1991.

Romanov, S. A.: A Correlation Analysis of Vector Variables as Ap-
plied to the Study of ELF Interplanetary Plasma Waves, Cosmic
Research, 36, 4, 339–354, 1998.

Romanov, V., Savin, S., Klimov, S., Romanov, S., Yermolaev, Yu.,
Blecki, J., and Wronowski, R.: Magnetic turbulence at the mag-
netopause: plasma penetration, J. Tech. Phys. (Poland), 40, 1,
329–332, 1999.

Russell, C. T.: The structure of the magnetopause, in: Physics of
the Magnetopause, edited by Song, P., Sonnerup, B. U. O., and
Thomsen, M. F., pp. 81–98, American Geophysical Union, 1995.

Russell, C. T., Snare, R. C., Means, J. D., Pierce, D., Dearborn, D.,
et al.: The GGS Polar magnetic fields investigation, Space Sci.
Res, 21, 563–582, 1995.

Russell, C. T., Fedder, J. A., Slinker, S. P., Zhou, X. W., Le, G.,
et al.: Entry of the POLAR spacecraft into the polar cusp under
northward IMF conditions, Geophys. Res. Lett., 25, 3015, 1998.

Safrankova, J., Nemecek, Z., Sibeck, D., Prech, L., Merka, J., and
Santolik, O.: Two-point observation of high-latitude reconnec-
tion, Geophys Res. Lett., 25, 4301–4304, 1998.

Sandahl, I., Popielavska, B., Budnick, E. Yu., Fedorov, A., Savin,
S., Safrankova, J., and Nemecek, Z.: The cusp as seen from
INTERBALL, Proceedings of 'Cluster II Workshop. Multi-
scale/Multipoint Plasma Measurements, Imperial College, Lon-
don, Sept. 22–24, 1999, ESA/ SP-499, p. 39–45, 2000.

Savin, S. P.: ELF waves near the high latitude magnetopause, in:
Abstracts of AGU Chapman Conference on Physics of the Mag-
netopause, March 14–18, 41, 1994.

Savin, S. P., Balan, O., Borodkova, N., Budnik, E., Nikolaeva,
N., Prokhorenko, V., Pulkkinen, T., et al.: Interball Magnetotail
Boundary Case Studies, Adv. Space Res., 19, 993, 1997.

Savin, S. P., Romanov, S. A., Fedorov, A. O., Zelenyi, L., Klimov,
S. I., et al.: The cusp/magnetosheath interface on 29 May 1996:
Integball-1 and Polar observations, Geoph. Res. Lett., 25, 2963–
2966, 1998a.

Savin, S. P., Borodkova, N. L., Budnik, E. Yu., Fedorov, A. O.,
Klimov, S. I., et al.: Interball tail probe measurements in outer
cusp and boundary layers, in: Geospace Mass and Energy Flow:
Results from the International Solar-Terrestrial Physics Program,
edited by Horwitz, J. L., Gallagher, D. L., and Peterson, W.

K., Geophysical Monograph 104, American Geophysical Union,
Washington D.C., pp. 25–44, 1998b.

Savin, S., Zelenyi, L., Budnik, L., Borodkova, N., Fedorov, A., et
al.: Manifestations of Boundary Layer Dynamics in Substorm
Activity. Multi Spacecraft Study, in: SUBSTORM-4, Interna-
tional Conference on Substorms-4', Lake Hamana, Japan: March
9-13, 1998, edited by Kokubun, S. and Kamide, Y., pp. 125–130,
Terra Scientific Publ. Co., Tokyo, 1998c.

Savin, S., Budnik, E., Nozdrachev, M., Romanov, V., et al.: On the
plasma turbulence ant at the polar cusp outer border, Chekhoslo-
vak J. Phys., 49, 4a, 679–693, 1999.

Savin S. P., Zelenyi, L. M., Romanov, S. A., Klimov, S. I., Skalsky,
A. A., et al.: Turbulent Boundary layer at the Border of Geomag-
netic Trap, JETP Letters, 74, 11, 547–551, 2001.

Savin, S., Zelenyi, L., Maynard, N., Sandahl, I., Kawano, H., Rus-
sell, C. T., et al.: Multi-spacecraft Tracing of Turbulent Boundary
Layer, Adv. Space Res., 30, 12, 2821–2830, 2002a.

Savin, S., Büchner, J., Consolini, G., Nikutowski, B., Zelenyi, L.,
Amata, E., et al.: On the properties of turbulent boundary layer
over polar cusps, Nonlin. Proc. Geophys., 9, 443–451, 2002b.

Sibeck, D. G., Lopez, R. E., and Roelof, E. C.: Solar wind control of
the magnetopause shape, location and motion. J. Geophys. Res.,
96, 5489–5495, 1991.

Smith, M. F. and Lockwood, M.: Earth's magnetospheric cusps,
Rev. Geophys., 34, 233, 1996.

Spreiter, J. R. and Stahara, S. S.: A new predictive model for de-
termining solar wind- terrestrial planet interactions, J. Geophys.
Res., 85, 6769–6777, 1980.

Spreiter, J. R. and Briggs, B. R.: Theoretical determination of the
form of the boundary of the solar corpuscular stream produced
by interaction with the magnetic dipole field of the Earth, J. Geo-
phys. Res., 67, 37–51, 1962.

Stasiewicz, K., Seyler, C. E., Gustafsson, G., Pickett, J., and
Popielawska, B.: Magnetic Bubbles and Kinetic Alfvén Waves
in the High-Latitude Magnetopause Boundary; J. Geophys. Res.,
106, 29 503, 2001.

Treumann, R. A., Labelle, J., and Bauer, T. M.: Diffusion processes:
an observational perspective, in: Physics of the magnetopause,
edited by Song, P., Sonnerup, B. U. O., and Thomsen, M. F., p.
331, American Geophysical Union, 1995.

Urquhart, A. L., Reiff, P. H., Toffoletto, F. R., Hill, T. W., Konkel, T.
R., et al: Polar magnetopause crossing of May 29, 1996: Implica-
tion for magnetic field modeling, J. Geophys. Res., 103, 17 323–
17 332, 1998.

Vaisberg, O. L., Galeev, A. A., Zeleny, L. M., Zastenker, G. N.,
Omelchenko, A. N., Klimov, S. I., Savin, S. P., et al.: Fine struc-
ture of the magnetopause from the measurements of the satel-
lites PROGNOZ-7 and PROGNOZ-8, Cosmic Research, (Transl.
from Russian), 21, 49, 1983.

Yamauchi, M. and Lundin, R.: The Wave-Assisted Cups Model:
Comparison to Low-Latitude Observations, Phys. Chem. Earth,
22, 729–734, 1997.

Zelenyi, L. M. and Milovanov, A. V.: Multiscale magnetic struc-
ture of the distant tail: self-consistent fractal approach, in: New
Perspectives on the Earth Magnetotail, Geophysical Monograph
105, AGU, Washington D.C., pp. 321–338, 1998.

Zhou, X.-W. and Russell, C. T.: The location of the high latitude
polar cusp and the shape of the surrounding magnetopause, J.
Geophys. Res., 102, 105–110, 1997.